JGR Atmospheres

RESEARCH ARTICLE
10.1029/2021JD035925

Special Section:
Fire in the Earth System

Australian Fire Emissions of Carbon Monoxide Estimated by Global Biomass Burning Inventories: Variability and Observational Constraints

Maximilien J. Desservettaz[1,2,3], Jenny A. Fisher[1], Ashok K. Luhar[2], Matthew T. Woodhouse[2], Beata Bukosa[4], Rebecca R. Buchholz[5], Christine Wiedinmyer[6], David W. T. Griffith[1], Paul B. Krummel[2], Nicholas B. Jones[1], Nicholas M. Deutscher[1], and Jesse W. Greenslade[1,7]

[1]Centre for Atmospheric Chemistry, School of Earth, Atmospheric and Life Sciences, University of Wollongong, Wollongong, NSW, Australia, [2]Climate Science Centre, CSIRO Oceans & Atmosphere, Aspendale, VIC, Australia, [3]Now at the Climate & Atmosphere Research Centre, The Cyprus Institute, Nicosia, Cyprus, [4]National Institute of Water and Atmospheric Research, Wellington, New Zealand, [5]Atmospheric Chemistry Observations & Modeling Laboratory, National Center for Atmospheric Research, Boulder, CO, USA, [6]Cooperative Institute for Research in Environmental Sciences, University of Colorado Boulder, Boulder, CO, USA, [7]Now at the Bureau of Meteorology, Melbourne, VIC, Australia

Abstract Australian fires are a primary driver of variability in Australian atmospheric composition and contribute significantly to regional and global carbon budgets. However, biomass burning emissions from Australia remain highly uncertain. In this work, we use surface in situ, ground-based total column and satellite total column observations to evaluate the ability of two global models (GEOS-Chem and ACCESS-UKCA) and three global biomass burning emission inventories (FINN1.5, GFED4s, and QFED2.4) to simulate carbon monoxide (CO) in the Australian atmosphere. We find that emissions from northern Australia savanna fires are substantially lower in FINN1.5 than in the other inventories. Model simulations driven by FINN1.5 are unable to reproduce either the magnitude or the variability of observed CO in northern Australia. The remaining two inventories perform similarly in reproducing the observed variability, although the larger emissions in QFED2.4 combined with an existing high bias in the southern hemisphere background lead to large CO biases. We therefore recommend GFED4s as the best option of the three for global modeling studies with focus on Australia or the Southern Hemisphere. Near fresh fire emissions, the higher resolution ACCESS-UKCA model is better able to simulate surface CO than GEOS-Chem, while GEOS-Chem captures more of the observed variability in the total column and remote surface air measurements. We also show that existing observations in Australia can only partially constrain global model estimates of biomass burning. Continuous measurements in fire-prone parts of Australia are needed, along with updates to global biomass burning inventories that are validated with Australian data.

Plain Language Summary Biomass burning inventories estimate the distribution and abundance of gases emitted to the atmosphere from fires. In this study, we found that three popular fire emission inventories (GFED, FINN, and QFED) predict very different emissions of the gas carbon monoxide (CO) from fires in Australia. To determine which inventory is best for Australia, we fed those emissions into global atmospheric models that combine the emissions with the chemistry and movement of gases in the atmosphere to predict the abundance of atmospheric gases, including CO. We compared the predictions to measurements in the real atmosphere. We found that GFED is better suited for Australian studies than QFED, which led to large overestimates, or FINN, which failed to capture much of the annual variation in measured CO levels. To further the outcomes of this study, more ground-based measurements are needed in Australia, particularly in the northern half of the continent where most of the fires normally occur. In addition, the use of atmospheric models with finer resolution would also allow us to make better use of the existing ground-based measurements to judge the reliability of different fire emission inventories.

Key Points:

- GFED4s and QFED2.4 outperform FINN1.5, especially in northern savanna regions
- ACCESS-UKCA provides a better CO simulation near fresh emissions, while GEOS-Chem better captures variability in remote measurements
- Sparsity and locations of Australian ground-based measurements offer limited constraints on Australian fire emissions in global models

Supporting Information:

Supporting Information may be found in the online version of this article.

Correspondence to:

M. J. Desservettaz and J. A. Fisher,
m.desservettaz@cyi.ac.cy;
jennyf@uow.edu.au

Citation:

Desservettaz, M. J., Fisher, J. A., Luhar, A. K., Woodhouse, M. T., Bukosa, B., Buchholz, R. R., et al. (2022). Australian fire emissions of carbon monoxide estimated by global biomass burning inventories: Variability and observational constraints. *Journal of Geophysical Research: Atmospheres*, *127*, e2021JD035925. https://doi.org/10.1029/2021JD035925

Received 25 SEP 2021
Accepted 16 JAN 2022

1. Introduction

Emissions from biomass burning have a large influence on atmospheric composition in the Southern Hemisphere where, relative to the Northern Hemisphere, slash and burn practices, pasture maintenance and accidental fires are more common and emissions from fossil fuels are much lower (Wai et al., 2014). Australia contributes

approximately 5%–10% to global biomass burning carbon emissions, with contributions from savanna fires in the north and forest fires in the south (Prosperi et al., 2020; Shi et al., 2015; van der Werf et al., 2017). These estimates come from global biomass burning inventories parameterized based on measurements performed almost exclusively outside Australia (Akagi et al., 2011). However, Australian ecosystems are uniquely characterized by a large fraction of eucalyptus vegetation, unlike anywhere else in the world (Gill, 1975), with possible implications for simulation of smoke emissions from Australian fires (i.e., the pattern of burning and species emitted could be different). The accuracy of global biomass burning emission estimates for Australia has not previously been evaluated. Here, we perform a suite of global model simulations of atmospheric composition driven by three global biomass burning inventories with differing emissions from Australia. We evaluate these simulations with surface, total column and satellite observations of carbon monoxide (CO), which is a marker of the degree of smoke in the atmosphere, to assess the fidelity of the inventories as well as the capability of existing measurements to constrain modeled atmospheric composition in Australia.

Global biomass burning emission inventories are widely used as inputs to atmospheric chemistry models to link emissions to their impacts on atmospheric composition, air quality, health, and climate. Most inventories calculate the emissions from fires using some variant of the Seiler and Crutzen algorithm shown in Equation 1 (Seiler & Crutzen, 1980):

$$E_i = A \times L \times CC \times EF_i \quad (1)$$

where E_i is the estimated mass of species i emitted from biomass burning, calculated as the product of area burnt (A, area), fuel load (L, mass of fuel per area), combustion completeness (CC, unitless) and the emission factor for species i (EF_i, mass of species i emitted per mass of fuel burned). The area burnt is retrieved by satellite imagery. The fuel load is the amount of combustible vegetation per unit area and can be estimated from satellite data or be parameterized per vegetation type and region. The combustion completeness, also referred to as burning efficiency or fractional combustion, is the fraction of the total fuel load that is fully combusted and released to the atmosphere. It is usually modeled based on the type of vegetation burnt, the estimated fire intensity, and in some cases the soil moisture content and/or time since the area was last burnt (Giglio et al., 2013). In some inventories, satellite-derived fire radiative power combined with regional conversion factors is used as a proxy to estimate the amount of fuel combusted ($A \times L \times CC$) (Darmenov & da Silva, 2015; Wooster et al., 2005). The emission factors represent the fraction of the burnt fuel that is emitted as trace gas i. They are derived from laboratory and field measurements conducted using specific fuels or in specific ecosystems, and are compiled for broad land cover or vegetation type such as savanna or tropical forest (e.g., Akagi et al., 2011; Andreae, 2019; Andreae & Merlet, 2001).

Although most global inventories rely on some form of Equation 1, there are a number of variations in their input data sources and implementation that lead to significant differences in emission estimates (Carter et al., 2020; Liu et al., 2020; Pan et al., 2020). Inter-inventory differences are not globally consistent, and previous work has shown that variability between inventories is larger for Australia than for most of the rest of the world (Liu et al., 2020). This variability ultimately leads to large uncertainty in Australian atmospheric composition as simulated by models that use these inventories as input. Observations available to constrain these uncertainties are sparse, with only a handful of long-term trace gas measurement sites (including both remote sensing and surface in situ measurements) spread out across a continent roughly the size of the continental United States. Perhaps as a result, no previous work has attempted to evaluate the fidelity of different global inventories for simulating atmospheric composition in the Australian environment.

In this work, we address two fundamental questions for understanding the impact of Australian biomass burning on regional and global atmospheric composition: (1) *How much do current estimates of Australian biomass burning CO emissions vary, and what impact does that variation have on simulated CO abundance?* and (2) *Are existing observations sufficient to constrain these estimates?* To answer the former, we run a suite of model simulations using two global atmospheric chemistry models (GEOS-Chem and ACCESS-UKCA, see acronyms list for full names) with three separate global biomass burning inventories (GFED4s, FINN1.5, and QFED2.4) and quantify the resultant range in the magnitude and interannual variability of CO emissions, simulated CO mixing ratios in surface air, and simulated CO total columns. To address the latter, we compare the simulated CO to surface in situ, ground-based total column, and satellite CO observations and evaluate the performance of each simulation. In the following sections, we first describe the biomass burning emission inventories, global models,

and measurement datasets (Section 2). We then compare estimates of biomass burning emissions from each of the three inventories for Australia and contextualize these on hemispheric and global scales (Section 3). Finally, we evaluate the CO simulations using the Australian observations and make recommendations as to the most appropriate biomass burning emissions to use for simulating Australian atmospheric composition (Section 4).

2. Methodology

The evaluation was done for the period 2008–2010. This 3-year time frame was selected to encompass 2009, the year of the "Black Saturday" event which, until the summer of 2019–2020, was Australia's worst bushfire disaster on record. This event took place around February 7, 2009, and burnt 4,500 km^2 of forest in the south-eastern state of Victoria, claiming 173 lives and destroying more than 3500 buildings (Cruz et al., 2012). This major biomass burning event left a clear fingerprint on both atmospheric measurements and emission estimates (Paton-Walsh et al., 2012; Siddaway & Petelina, 2011). Thus, a 3-year window around the Black Saturday event was simulated to capture the impact of interannual variability on the results. We expect results from this period to be generally applicable to other years, including more recent years, as Paton-Walsh et al. (2022) showed that there has been no long-term trend in annual Australian fire CO emission estimated by any global inventory between 2003 and 2019.

We quantify the relative importance of variability in emission inventories versus variability in chemical transport model by using two global atmospheric chemistry models and three emission inventories. The impact of variability in emission inventories is quantified by running one model (GEOS-Chem) with all three inventories (GFED4s, FINN1.5, and QFED2.4). We note that another widely used biomass burning emission inventory, the Global Fire Assimilation System (GFAS, Kaiser et al., 2012), was not included as it was not implemented in the version of GEOS-Chem used in this study. The impact of model variability is quantified by running both models (GEOS-Chem and ACCESS-UKCA) with the same emission inventory (GFED4s). For the latter, we focus on the models' ability to simulate seasonal cycles, as ACCESS-UKCA emission inputs and trace gas outputs were only available at monthly resolution (see Section 2.2.2). Our goal is in part to identify the global modeling set-up available in existing models that provides the best simulation for CO in the Australian region. As such, we use each inventory at the best available temporal resolution implemented in each model (as described below). The inventories and models are described briefly below (Sections 2.1 and 2.2), along with the observations and statistical measures used to evaluate the model simulations (Section 2.3). Our analysis uses CO as the trace gas that is both measured at the most Australian observing sites and most sensitive to biomass burning emissions. Preliminary additional evaluation using formaldehyde and ethane (both measured at fewer stations than CO) provided no additional insights and therefore is not discussed further.

2.1. Biomass Burning Emission Inventories

2.1.1. GFED4s

The Global Fire Emissions Database version 4s (GFED4s) biomass burning emissions were used in both the GEOS-Chem model with 3-hourly resolution and in the ACCESS-UKCA model with monthly resolution (models described below). The difference in the temporal resolution of the emission inputs limits our inter-model comparison to monthly averages, as will be discussed further below. The GFED4s inventory is described in detail by van der Werf et al. (2017). In brief, the fuel loading in GFED4s is derived from the Carnegie-Ames-Stanford-Approach (CASA) biogeochemical model (Field et al., 1995; Potter et al., 1993; Randerson et al., 1996). The GFED4 burned area (without small fires) is obtained from the 500 m MODIS Collection 5.1 MCD64A1 burned area product (Giglio et al., 2013). For fires smaller than 21 ha (the size of the 500 × 500 m MODIS pixel), the direct mapping of the burned area is not reliable. Therefore, to account for smaller fires, active fires from MODIS and 500 × 500 m surface reflectance observations are combined with the MCD64A1 burned area product. The burned area of small fires is calculated by multiplying the number of active fires outside the perimeter of the MCD64A1 burned area by the ratio of burned area to active fires within the perimeter of the MCD64A1 burned area. The estimate of burned area for each small fire is refined by a correction factor to account for the region, vegetation type and season. Specific details of this approach are given by Randerson et al. (2012).

As detailed by van der Werf et al. (2017) and references therein, fuel load and combustion completeness are derived from the carbon cycle aspect inherited from CASA. The model dynamically adjusts the modeled amount of carbon in different carbon pools (such as stems, leaves and litter) using the fraction of absorbed

photosynthetically active radiation, a dataset derived from measurements by the Advanced Very High Resolution Radiometer (AVHRR) sensor on-board several satellites. Combustion completeness is set between minimum and maximum fractions depending on the land cover and then defined within those limits using soil moisture. Land cover types include evergreen needleleaf forests, evergreen broadleaf forests, deciduous needleleaf forests, deciduous broadleaf forests, mixed forests, closed shrublands, open shrublands, woody savannas, savannas, grasslands and croplands. Emission factors are from the inventory compilation by Akagi et al. (2011).

2.1.2. FINN1.5

The Fire INventory from NCAR version 1.5 (FINN1.5) biomass burning emissions, described in detail by Wiedinmyer et al. (2011), were used only as input to GEOS-Chem, with daily resolution. In FINN, the location and size of fires are derived from satellite detection of active fires only. Active fires are retrieved from the MODIS Thermal Anomalies Product daily, with a nominal resolution of 1 km^2. Fires detected with a confidence level of less than 20% are removed. In the tropics, between 30°N and 30°S, MODIS takes 2 days to achieve full coverage. Therefore, fires detected on one day are assumed to carry over to the following day at half their original size. Because there are two MODIS instruments, the possibility of double-counting fires is removed by discounting any hot spot detected within a 1-km radius of an existing fire detection each day.

The MODIS Collection 5 Land Cover Type supplies FINN1.5 with the type of vegetation burned in each pixel. Fourteen of the 16 land types in the MODIS dataset are lumped into six generic land cover classes: boreal forests, tropical forests, temperate forests, woody savannas and shrublands, savannas and grasslands and croplands. The remaining two, water and ice, are used to filter out any anomalous hot spots. The fraction of tree, non-tree vegetation and bare cover in each pixel is obtained from the MODIS Vegetation Continuous Fields product. The area burned is assumed to be 1 km^2 for each pixel, except for savanna and grassland areas, where it is assumed to be 0.75 km^2 (due to the lower vegetation density). The area burned values are further scaled using the MODIS Vegetation Continuous Field bare cover fraction in each pixel.

Fuel loading is set by region and generic land cover class based on Hoelzemann et al. (2004). For instance, the fuel density for savanna and grassland vegetation in Oceania is estimated at 245 g m^{-2}, which is approximately half the density estimated for the same land cover type in South America (552 g m^{-2}). This represents a significant difference from GFED4s and its dynamically calculated fuel loading. The combustion completeness is set depending on the tree cover with three options: tree cover below 40%, tree cover between 40% and 60%, and tree cover higher than 60%. As in GFED4s, emission factors are from Akagi et al. (2011).

2.1.3. QFED2.4

The Quick Fire Emission Dataset version 2.4 (QFED2.4) biomass burning emissions, described by Darmenov and da Silva (2015), were used only in GEOS-Chem, with daily resolution. In QFED, emissions are calculated based on fire radiative power, which quantifies the rate of radiant heat produced by a fire and has been shown to be linearly related to the mass of fuel consumed in a fire (Wooster, 2002). Fire radiative power and fire location are obtained from the MODIS Collection 5 Active Fire product (MOD14 and MYD14) and the MODIS Geolocation product (MOD03 and MYD03) with a 1 km^2 spatial resolution, up to four times each day. In the case of pixels obscured by clouds, QFED2.4 uses a technique called the sequential approach, which models a predicted value of fire radiative power from a previous measurement in the same pixel. This predicted value is then used to correct the observed fire radiative power with a scalar parameter, which depends on the quality of the sensor's retrieval.

The QFED vegetation map is then used to assign the vegetation type, select the relevant coefficient to convert fire radiative power to mass of dry fuel consumed, and select the relevant emission factors. The QFED vegetation map is derived from the International Geosphere-Biosphere Programme (IGBP), with improvements of the Brazilian tropical forests by the Brazilian National Institute For Space Research (IGBP-INPE), with 1 km^2 spatial resolution. The IGBP-INPE 17 land cover types are aggregated into four basic vegetation types used by QFED: tropical forest, extra-tropical forest, savanna and grassland. For each vegetation type, the fire radiative power-to-fuel consumption coefficients are based on comparison to GFEDv2. Emission factors are from Andreae and Merlet (2001), which for CO are ∼15% different for extratropical forest fires and almost identical for savanna fires to those reported by Akagi et al. (2011) (as used in the other two inventories).

Table S1 in Supporting Information S1 summarizes the three inventories' inputs for comparison. The emission factors are very similar between the different inventories. Most of the differences between inventories will most

likely be caused by the calculation methods, burn area or hot spot detection, detail of land classification, and assumptions made in the process to estimate emissions.

2.2. Chemical Transport Models

2.2.1. GEOS-Chem

We used the tropospheric chemistry ("tropchem") simulation of the GEOS-Chem (Bey et al., 2001) chemical transport model version 10-01 (http://wiki.seas.harvard.edu/geos-chem/index.php/GEOS-Chem_v10-01), driven by assimilated meteorological fields from the NASA Global Modelling and Assimilation Office Goddard Earth Observing System, Version 5 (GEOS-5) reanalysis data product. For global simulations as used here, the native GEOS-5 resolution of 0.5° latitude by 0.667° longitude by 72 vertical levels is downgraded for use in GEOS-Chem to 2° latitude by 2.5° longitude by 47 vertical levels. The model uses a hybrid sigma pressure vertical grid. The vertical resolution decreases with height, with up to 38 levels in the troposphere. The tropopause is calculated dynamically, and so the number of levels in the troposphere varies. Only purely stratospheric levels are lumped when downgrading the resolution from 72 to 47 vertical levels.

The model was run from 2008 to 2010. A 6-month spin-up preceded the period of interest to allow the model's chemistry to reach equilibrium. The model calculates CO online using the full tropospheric chemistry chemical mechanism. Previous analyses have shown that GEOS-Chem OH compares well to observations (Travis et al., 2020) and produces a methane lifetime within the range simulated by other models (Nicely et al., 2017, 2020). Model timesteps were 15 min for convection and transport and 30 min for emissions and chemistry. Model output was saved with hourly resolution at the measurement sites and monthly resolution everywhere else.

Biomass burning emissions (described above) were emitted into the model surface layer. The height of the first model layer in GEOS-Chem varies depending on surface pressure, but on average is centred at 65 m above ground level (Travis & Jacob, 2019). Anthropogenic emissions were from the Emission Database for Global Atmospheric Research (EDGARv4.2; Olivier et al., 2002) for CO, nitrogen oxides, sulfur dioxide and ammonia and the REanalysis of the TROpospheric chemical composition (RETRO; Reinhart & Millet, 2011) for volatile organic compounds. We use the most recent available emissions from each inventory (2008 for EDGAR and 2000 for RETRO). These were supplemented with biofuel emissions from Yevich and Logan (2003), aircraft emissions from the Aviation Emissions Inventory Code (AEIC; Simone et al., 2013) and ship emissions from the International Comprehensive Ocean Atmosphere Data Set (ICOADS; Woodruff et al., 2011) for CO and nitrogen oxide and from the Arctic Research of the Composition of the Troposphere from Aircraft and Satellites inventory (ARCTAS; Eyring et al., 2005) for sulfur dioxide. Biogenic emissions were from the Model of Emissions of Gases and Aerosols from Nature v2.1 (MEGANv2.1; Guenther et al., 2012), calculated online in GEOS-Chem.

2.2.2. ACCESS-UKCA

We used the ACCESS-UKCA chemistry-climate model, which combines the physical atmosphere from the United Kingdom Met Office's Unified Model version 8.4 with the UKCA chemistry model (Abraham et al., 2012; Bi et al., 2013; Woodhouse et al., 2015, http://www.ukca.ac.uk). In the model setup used here, ACCESS is essentially the same as the Unified Model since the ACCESS-specific ocean and land-surface components are not invoked. The model is run in atmosphere-only mode with prescribed monthly mean sea surface temperature and sea ice fields, and the UM's original land-surface scheme (Joint UK Land Environment Simulator; JULES) is used. The UKCA configuration used here combines both tropospheric and stratospheric chemistry schemes. The total number of reactions, including aerosol chemistry, is 306 across 86 species.

The atmospheric model has a horizontal resolution of 1.875° in longitude and 1.25° in latitude, and 85 staggered terrain-following hybrid-height levels extending from the surface to 85 km. The vertical resolution decreases with height, with the lowest 65 levels (up to ~30 km) lying within the troposphere and lower stratosphere.

The model's meteorological fields (horizontal wind components and potential temperature) were nudged to ECMWF's ERA-Interim reanalyses (Dee et al., 2011) on pressure levels in the free troposphere. The model output used here was extracted from a longer model run starting from 1997. Because the model was not run specifically for this work, only monthly mean model output was available. The monthly time resolution of both the input emissions and the model output for ACCESS-UKCA hinders our ability to compare the ACCESS-UKCA model to the observations and to GEOS-Chem at sub-monthly resolution. Instead, we use the ACCESS-UKCA output

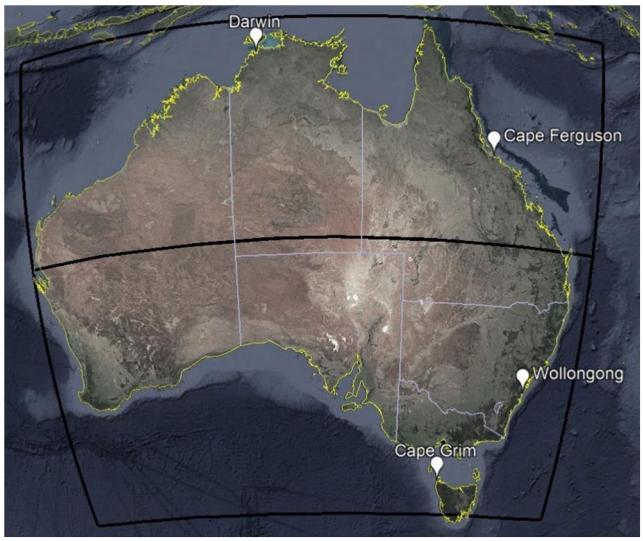

Figure 1. Location of the ground-based measurements sites: Darwin (12.5°S, 130.8°E), Cape Ferguson (19.3°S, 147.1°E), Wollongong (34.4°S, 150.9°E), and Cape Grim (40.7°S, 144.7°E). The black lines delimit the northern and southern Australian regions (separated by 25°S) referred to in this study. Satellite image from Google Earth (Landsat/Copernicus).

for monthly comparisons only, allowing us to quantify the performance of the different models for simulating the CO seasonal cycles.

Biomass burning emissions were from GFED4s (described above) with CO emitted into the model surface layer. Over land, the height of the first model layer in ACCESS-UKCA varies depending on topography, with thickness of 20 m over the ocean, but compressed over land. Anthropogenic emissions were from the Atmospheric Chemistry and Climate Model Intercomparison Project (ACCMIP; Lamarque et al., 2013). Biogenic emissions were from the MEGAN – Monitoring Atmospheric Composition and Climate project (MEGAN-MACC; Sindelarova et al., 2014). A detailed description of the ACCESS-UKCA simulation as used here is presented in Woodhouse et al. (2015).

2.3. Observations

To evaluate the two atmospheric models over Australia using the three estimates of biomass burning emissions, we used a suite of CO observations from surface in situ data, ground-based total column data, and satellite-based measurements from the Measurements Of Pollution In The Troposphere (MOPITT) instrument onboard NASA's Earth Observing System Terra spacecraft. For comparison to the observations, GEOS-Chem was sampled with hourly resolution at the locations of the ground-based stations using the *Station Diagnostic (ND48)*, a model diagnostic designed for comparing model output to surface-based observations.

Figure 1 shows the locations of the four Australian sites where ground-based in situ and/or total column CO observations were available: Darwin (Northern Territory), Cape Ferguson (Queensland), Wollongong (New South Wales), and Cape Grim (Tasmania). Surface in situ data were available for all sites except Wollongong, for which only total column data were consistently available during the study period. All data providers apply quality control to their datasets before release, and we do not apply any further quality control measures here. Data coverage for online in-situ observations is visualized in Figure S8 in Supporting Information S1. At Darwin, surface in situ measurements were made using a Fourier Transform InfraRed (FTIR) spectrometer with 3-min resolution. The instrumental setup is presented by Griffith et al. (2012). At Cape Ferguson, in situ CO was sampled in flasks with approximately weekly resolution and analyzed by gas chromatography with mercuric oxide reduction detector (Langenfelds et al., 2002). At Cape Grim, in situ CO was sampled every 40 min by gas chromatography with a mercuric oxide reduction detector (Prinn et al., 2018). The Cape Ferguson data is available from the World Data Centre for Greenhouse Gases (WDCGG), part of the Global Atmospheric Watch program of the World Meteorological Organisation (Krummel et al., 2016). The Cape Grim data were provided directly by the Commonwealth Scientific and Industrial Research Organisation (CSIRO). For comparison to the models, the surface in situ observations were averaged to both hourly and monthly resolution.

Ground-based measurements of total column CO were made at Wollongong and Darwin using high-resolution solar FTIR spectrometers. Total column CO measurements were from the Network for the Detection of Atmospheric Composition Change (NDACC; http://www.ndsc.ncep.noaa.gov/) at Wollongong and the Total Column Carbon Observing Network (TCCON; http://www.tccon.caltech.edu/) at Darwin (GGG2014; Griffith et al., 2014; Wunch et al., 2011). Zhou et al. (2019) found that TCCON and NDACC CO agreed within 2% at sites in the Southern Hemisphere (including Wollongong). The time resolution of both instruments is approximately 1 min, and measurements are only made under daytime, cloud-free conditions. This resulted in clear annual lows and highs in data coverage at Darwin, due to the wet season (see Figure S9 in Supporting Information S1). For comparison to GEOS-Chem model output, the total column datasets, including averaging kernels and a priori profiles provided as part of the dataset, were averaged to hourly time resolution, and comparisons were made only for hours with available measurements. Modeled vertical profiles were extrapolated to the instrument's vertical levels and converted to partial columns. Instrumental averaging kernels and a priori profiles were then applied to the model partial columns and the smoothed partial columns summed to calculate smoothed model total columns that account for instrument sensitivity (Rodgers & Connor, 2003). Likewise, the total column datasets were also

Table 1
Australian Biomass Burning CO Emission Estimates

Region	Year	CO emissions (Tg)		
		FINN1.5	GFED4s	QFED2.4
Northern Australia[a]	2008	1.2	8.9	16
	2009	2.1	13.	22
	2010	0.7	4.8	8.7
Southern Australia[b]	2008	0.5	0.8	1.7
	2009	1.8	3.0	3.0
	2010	1.8	1.2	2.4
Australian total	2008	1.7	9.7	18
	2009	3.9	16.	25
	2010	2.5	6.0	11

[a]North of 25°S. [b]South of 25°S.

averaged monthly to account for instrument sensitivity when comparing with the ACCESS-UKCA model output (available at monthly resolution only).

To provide broader regional context on seasonal timescales, monthly mean model output was also compared to MOPITT Version 7 level 3 monthly data, obtained from the NASA data archive (ftp://l5eil01.larc.nasa.gov/MOPITT/MOP03JM.007, NASA/LARC/SD/ASDC, n.d.). The joint/multispectral TIR-NIR product was used, which, with the inclusion of solar reflectance, improves near-surface retrievals (Worden et al., 2010). The level 3 product of the nadir-sounding MOPITT instrument has a 1° × 1° horizontal resolution with global coverage over approximately 3 days (Deeter et al., 2017; Drummond & Mand, 1996; Emmons et al., 2009). The CO retrieval provides one to two independent pieces of information in the vertical. MOPITT uses correlation infrared radiometry, a technique that uses a cell on-board the instrument containing CO as reference. The internal length and pressure of this cell are modulated to gain spectral information. Buchholz et al. (2017) validated MOPITT CO using data from the NDACC network, including from Wollongong. They found MOPITT to slightly overestimate CO compared to ground-based FTIR (<10%) but did not find any significant latitude-dependent bias. Similarly, Hedelius et al. (2019) compared v7 MOPITT to TCCON and showed MOPITT was higher by 6%–8%.

Similar to the ground-based total columns, MOPITT instrumental averaging kernels and a priori profiles were applied to the model output to account for instrumental sensitivity. MOPITT data and smoothed model output were then averaged spatially over the northern and southern Australia regions shown in Figure 1. The 25°S latitude was chosen as the boundary between the northern and southern Australia regions following Buchholz et al. (2018) as: (1) it marks a dramatic change in rainfall and fire hotspot distributions (Russell-Smith et al., 2007); (2) it roughly coincides with the Tropic of Capricorn that divides tropical from temperate regions; and (3) it separates Australia's more populous south from the sparsely populated north (about 85% of the Australian population lives south of 25°S).

For all datasets, model-observation agreement was quantified by calculating the mean bias (*MB*, Equation 2) and the Pearson correlation coefficient (*r*) for each simulation compared to the relevant measurement dataset:

$$MB = \frac{\sum_{i=1}^{N}(M_i - O_i)}{N} \quad (2)$$

where N is the number of data points and M and O are the model and observed parameters respectively. The mean bias represents the average difference between the model output and observation. The correlation coefficient quantifies the strength of the linearity between model outputs and observation and is indicative of the model ability to reproduce the observed variability.

3. Biomass Burning Emission Estimates

3.1. Australian Emissions

Table 1 presents the total estimated CO emissions from Australian biomass burning as calculated from the GEOS-Chem ouptut with each inventory in each simulation year, separated into northern and southern Australian contributions (Figure 1). The spatial distribution of CO emissions is shown in Figure 2 for the year 2009 as an example, with total emissions from GFED4s (Figure 2a) compared to FINN1.5 (Figure 2b) and QFED2.4 (Figure 2c). All three inventories show emissions from savanna fires in the north and forest fires in the southeast, with the northern savanna fires the dominant emission source.

The total annual Australian biomass burning CO emissions vary by up to an order of magnitude between inventories. Emissions are lowest in FINN1.5 (1.7–3.9 Tg), followed by GFED4s (6–16 Tg), with the largest emissions from QFED2.4 (11–25 Tg). Liu et al. (2020) compared five biomass burning inventories, including the three of this study, and also found FINN (v1.5) and QFED (v2.5r1) to be the extreme cases for Australia when averaged

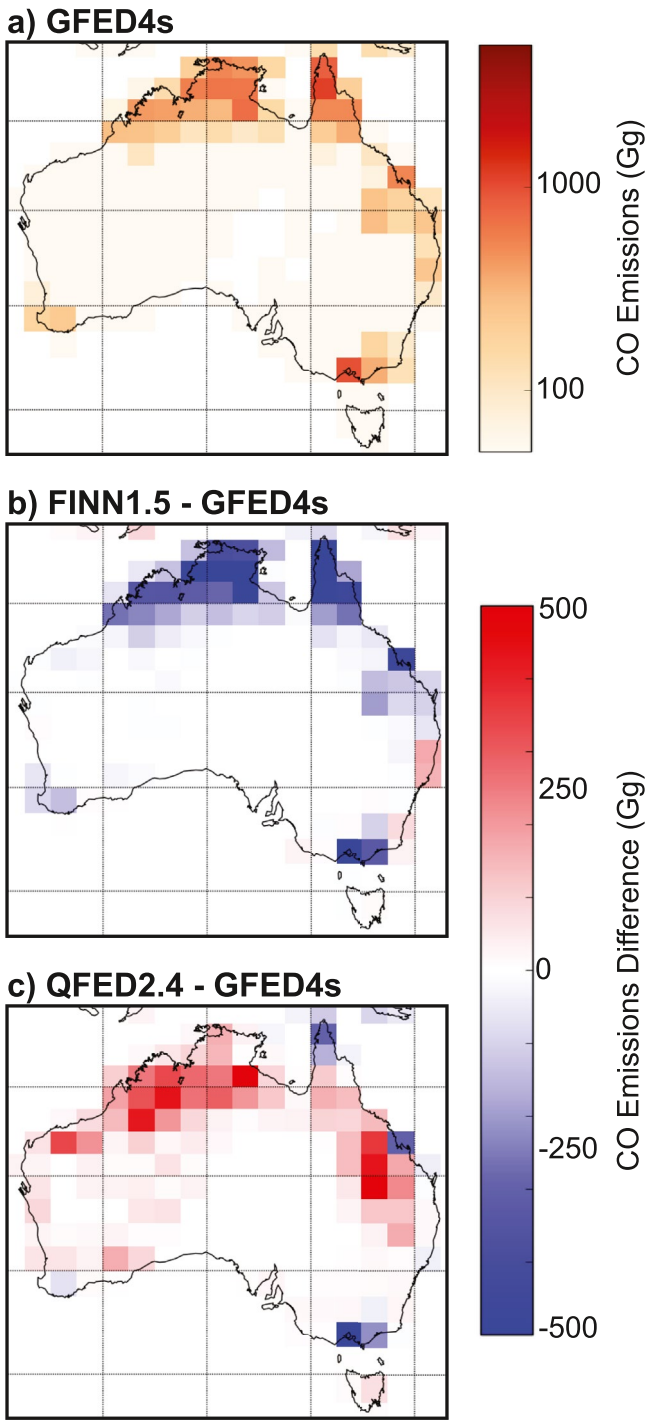

Figure 2. (a) CO emissions (Gg) over Australia in 2009 from GFED4s, along with the absolute differences between (b) FINN1.5 and GFED4s and (c) QFED2.5 and GFED4s.

over 2003–2016. Figure 2 shows that emissions from FINN1.5 are lower than GFED4s throughout Australia, while emissions from QFED2.4 are higher than GFED4s over the savanna regions but lower over the forest regions (both tropical and temperate). Given that FINN1.5 and GFED4s use the same emissions factors (see Section 2.1.1) and that the QFED2.4 emission factors are nearly identical for savannas and slightly higher for forests (see Table S1 in Supporting Information S1), we expect these differences to be driven by fire detection, assumed burned area and fuel consumption (rather than emission factors).

The inventories differ most significantly for the savanna fires in northern Australia. In both GFED4s and QFED2.4, the northern Australian emissions dominate the total Australian emissions budget, responsible for 4.8–13 Tg CO (76%–89% of the Australian total) in GFED4s and 8.7–22 Tg CO (79%–88% of the Australian total) in QFED2.4. These results are consistent with previous estimates that 83% of Australian biomass burning emissions originate from savanna fires (Shi et al., 2015). FINN1.5 emissions, on the other hand, are very low in northern Australia at only 0.7–2.1 Tg CO. The savanna fire emissions in FINN1.5 dominate the total Australian fire emissions only in 2008; in other years they account for only 28%–53% of the total.

The inventories also differ in their representations of interannual variability. Summed over both regions, FINN1.5 emissions are lowest in 2008, while GFED4s and QFED2.4 both show the lowest emissions in 2010. All three inventories show the largest emissions in 2009, both in the southern Australia region affected by the Black Saturday fires and in the northern Australia savanna region.

Figure 3 shows the time series of monthly mean CO emissions estimated by each inventory for northern and southern Australia (note the difference in scales). In northern Australia, GFED4s and QFED2.4 show that the largest emission peaks occur from September to December each year during the tropical dry season (Edwards et al., 2006), although only QFED2.4 shows a distinct peak in the latter half of 2010. FINN1.5 does not show any northern Australia seasonal CO increase in 2008 and 2010 and only a very small enhancement in 2009.

In southern Australia, CO emissions peak during austral summer (December to February), as shown in Figure 3. GFED4s and to a lesser extent QFED2.4 show a peak in southern Australia CO emissions in February 2009, coincident with the Black Saturday event. FINN1.5 does not show any enhancement during this event but does show significant peaks in October 2009 and March 2010 that are not seen in the other inventories.

3.2. Continental, Hemispheric and Global Emissions

To contextualize the Australian emissions, we also compare the inventory estimates for other Southern Hemisphere continents and at hemispheric and global scales. Table 2 presents annual total biomass burning CO emissions estimates for Australia, Africa, South America and South-East Asia (all south of the equator), the Southern Hemisphere, and the global total. Figure 4 shows the time series of the emission estimates for each region.

The three inventories agree well at the hemispheric scale, with mean annual emissions of 177 Tg (FINN1.5), 141 Tg (GFED4s), and 188 Tg (QFED2.4) in the Southern Hemisphere. However, this agreement masks differences at the continental scale that operate in different directions. While Australian emissions are significantly lower in FINN1.5 than in other inventories, South American emissions are higher in FINN1.5 for two of the

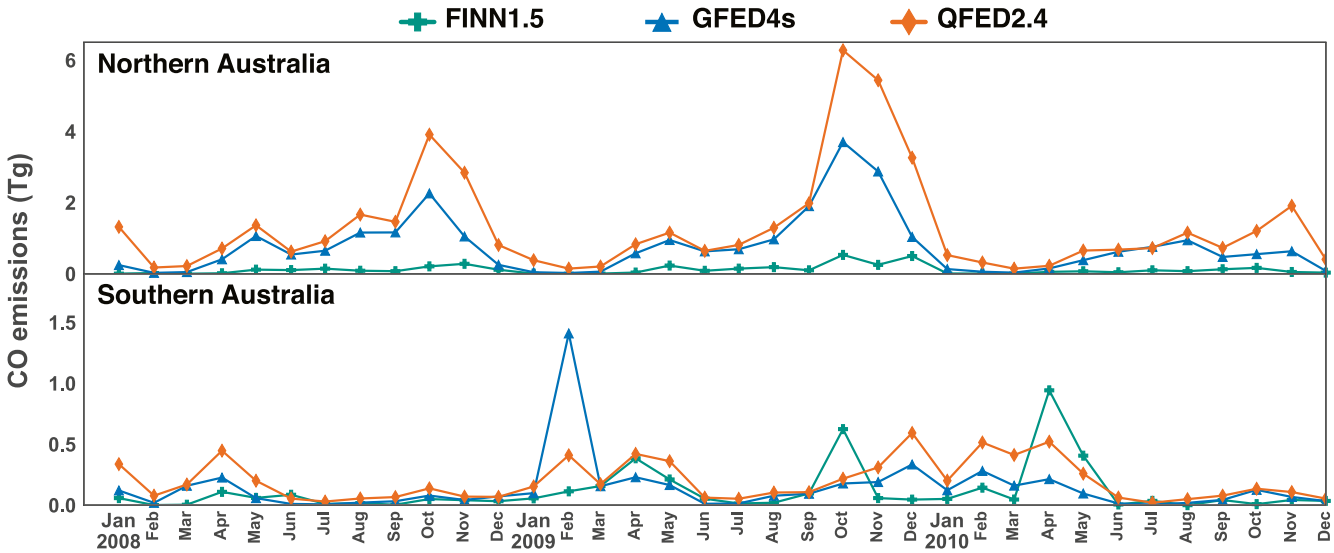

Figure 3. Biomass burning CO emissions (Tg) for northern (top) and southern (bottom) Australia as estimated by FINN1.5 (teal), GFED4s (blue), and QFED2.4 (orange) from January 2008 to December 2010. Note the difference in scales between the top and bottom panels.

three years. The three inventories agree best over Southern Hemisphere Africa, with GFED4s and QFED2.4 agreeing within 5%–15% of one another while FINN1.5 is 15%–45% lower than GFED4s.

Table 2
Annual CO Emissions (Tg) Obtained From the Three Inventories for Southern Hemisphere Regions and the Globe[a]

		CO emissions (Tg)		
		FINN1.5	GFED4s	QFED2.4
Australia	2008	1.6	10	18
	2009	3.9	16	25
	2010	2.5	6.0	11
Africa[b]	2008	79	96	107
	2009	66	95	101
	2010	56	103	117
South America[b]	2008	70	33	51
	2009	51	17	35
	2010	67	102	81
South-East Asia[b]	2008	3.9	2.7	5.5
	2009	17	49	8.1
	2010	4.0	1.6	5.8
Southern Hemisphere	2008	141	154	181
	2009	178	138	170
	2010	213	130	214
Global	2008	327	298	365
	2009	297	318	335
	2010	299	353	369

[a]Emissions are calculated from the GEOS-Chem output. [b]South of the equator.

Figure 4 shows that there are seasonal and interannual differences between the inventories. For the Southern Hemisphere Africa region, the start of the burning season is one month later in FINN1.5 than in the other inventories. In GFED4s and QFED2.4, there is little year-to-year difference in the seasonal emission maximum, whereas FINN1.5 predicts lower peak emissions in 2010 than in prior years.

Compared with Africa, the inventories show more interannual variability in the Southern Hemisphere South America region. All three inventories predict lower emissions in 2009 and higher emissions in 2010 (coincident with major fires in Bolivia and Brazil; Lewis et al., 2011), with 2008 intermediate in GFED4s and QFED2.4 but on par with 2010 in FINN1.5. In general, QFED2.4 and GFED4s emissions estimates in this region are quite similar in both magnitude and timing, although the annual decline from September to October is more rapid in GFED4s. During the South American fires in August-September 2010, GFED4s estimates are roughly 30% higher than those from QFED2.4. As was the case in Africa, the start of the South American burning season is delayed in FINN1.5 relative to the other inventories. FINN1.5 does not appear to capture the large August-September 2010 emission enhancement associated with the Bolivian and Brazilian fires, but does show an unexplained large peak in October 2010.

As shown in Figure 4, the variability on the hemispheric scale is almost exclusively driven by the variability in the African and South American emissions. One exception is the GFED4s peak in September 2009, which can be attributed to Indonesian fires. In general, emissions from Australia are dwarfed by those from Africa and South America, with Australia responsible for between 1% (FINN1.5 in 2008 and 2010) and 15% (QFED2.4 in 2009) of the hemispheric total. This small contribution combined with the long CO atmospheric lifetime (2–6 months; Khalil & Rasmussen, 1984) complicates the evaluation of the inventories using Australian CO observations, as will be discussed below.

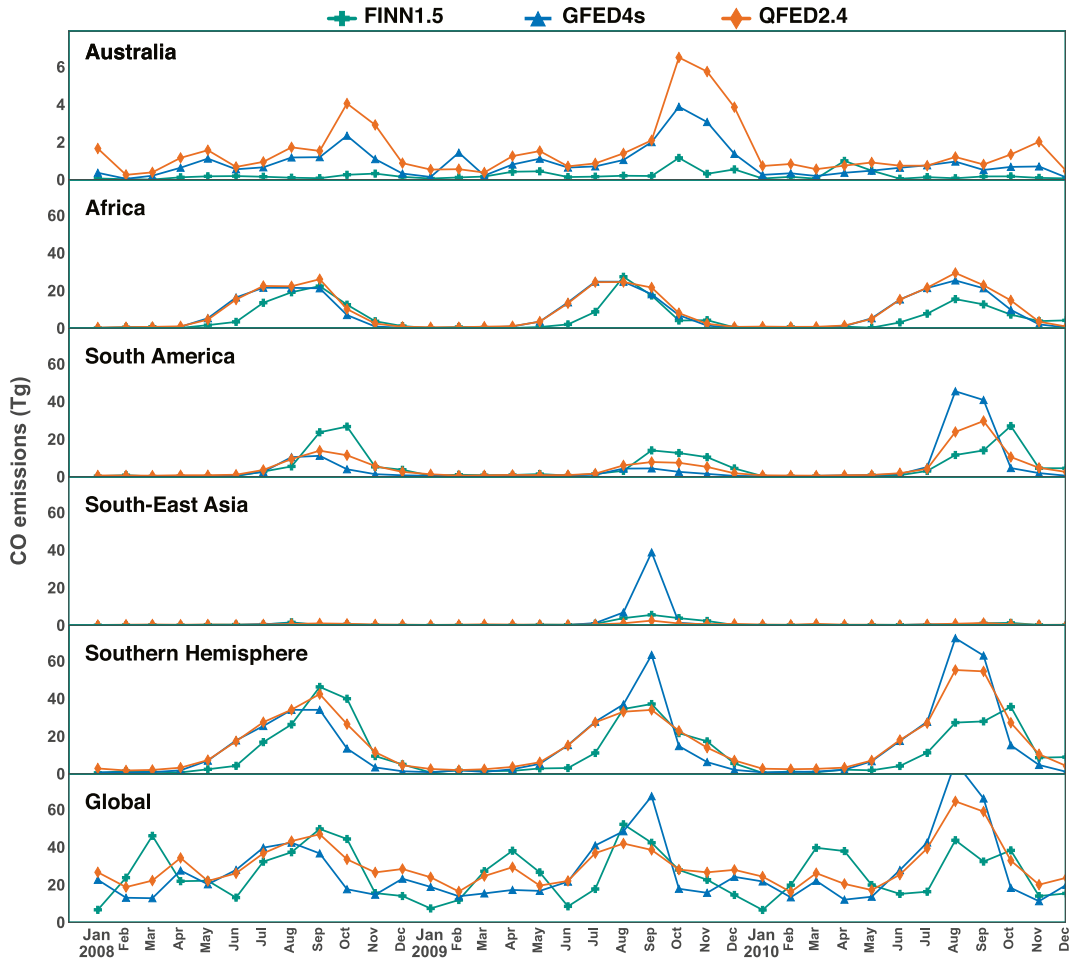

Figure 4. CO emissions (Tg) from biomass burning in (top to bottom) Australia, Africa, South America, South-East Asia, the Southern Hemisphere and the global total, as estimated by FINN1.5 (teal), GFED4s (blue), and QFED2.4 (orange) from January 2008 to December 2010. For the continental totals, only the regions south of the equator are included. Note the scale differences between Australia and all other regions.

4. Simulated CO at Australian Measurement Sites

As shown in the previous section, the estimates of Australian biomass burning emissions differ substantially between the GFED4s, FINN1.5, and QFED2.4 inventories. In this section, we evaluate the impact of these different emission estimates on simulated CO mixing ratios in the Australian region. We compare the model output to a suite of Australian atmospheric observations (described in Section 2.3) to test whether existing observations are sufficient to constrain the biomass burning emission estimates and, if so, determine which inventories provide the most accurate simulation of CO observed over Australia.

4.1. Northern Australia

We first compare simulated CO to surface in situ mixing ratios observed at Darwin and Cape Ferguson and to total column observations at Darwin (see Figure 1 for locations). Model evaluation using surface in situ observations provides information about model/inventory ability to reproduce specific fire events if these occur in the vicinity of the site, as most emissions (including those from low-intensity fires) are released within the planetary boundary layer. This is especially true at Darwin, which is located in close proximity to savanna fires and has previously been shown to regularly sample smoke from these fires (Cook et al., 1995; Desservettaz et al., 2017; Hurst, Griffith, Carras, et al., 1994; Hurst, Griffith, & Cook, 1994; Paton-Walsh et al., 2010). Cape Ferguson, on the other hand, is a more remote site, and surface in situ measurements here tend to be more representative

Table 3
Mean Bias Between the Modeled and Measured Surface CO Mixing Ratios and Total Columns in Northern Australia[a,b]

	GEOS-Chem			ACCESS-UKCA
	FINN1.5	QFED2.4	GFED4s	GFED4s
Surface in situ (ppbv)				
Darwin (observed mean = 157.6)				
Hourly data	−69.6 (−44%)	−36.9 (−23%)	−50.4 (−32%)	
Monthly mean	−69.4 (−44%)	−36.8 (−23%)	−50.0 (−32%)	−2.5 (−2%)
Cape Ferguson				
Hourly data	10.6 (17%)	24.1 (38%)	12.9 (21%)	
Monthly mean	12.3 (20%)	24.0 (38%)	14.6 (23%)	16.1 (26%)
Total Column (10^{18} molec cm^{-2})				
Darwin (observed mean = 1.52)				
Hourly data	0.079 (5%)	0.269 (18%)	0.153 (10%)	
Monthly mean	0.057 (4%)	0.247 (16%)	0.133 (9%)	0.248 (16%)
MOPITTc (observed mean = 1.45)				
Monthly mean	0.102 (7%)	0.236 (17%)	0.126 (9%)	0.138 (10%)

[a]See Figure 1 for locations. [b]Note that while the model timesteps are sub-hourly and the same for each simulation, the input emissions have different temporal resolutions as follows: FINN1.5 – daily, QFED2.4 – daily, GEOS-Chem/GFED4s – 3-hourly, ACCESS-UKCA/GFED4s – monthly. See Section 2 for further details. [c]Averaged over the full northern Australia region shown in Figure 1.

of northern Australia background air (Buchholz et al., 2016). Evaluation using the total column data provides complementary information on model simulation of regional air mass characteristics, with the column measurements less sensitive to local emissions and variations in the boundary layer mixing height than measurements made at the surface (Deutscher et al., 2010; Zeng et al., 2015). The integrated nature of the total column measurements can make them more appropriate for comparison to global models with coarse resolution (including those used here), but also makes them more sensitive to variations in emissions from distant sources (Keppel-Aleks et al., 2012).

We first quantify overall simulation performance using the mean bias relative to each observed dataset. Table 3 shows the mean bias of each simulation (GEOS-Chem with all three inventories and ACCESS-UKCA with GFED4s) in northern Australia. For each dataset, the bias has been calculated using both the original hourly data (shown in Figure 5) and the data averaged to monthly resolution, with only the latter available for the ACCESS-UKCA output. The mean bias relative to MOPITT satellite observations averaged over the full northern Australia region is also included in Table 3.

The mean biases in Table 3 provide a consistent picture: the models underestimate CO in the vicinity of fresh local emissions (Darwin surface in situ) but overestimate regional background CO (Cape Ferguson surface in situ, Darwin and MOPITT total columns). The three GEOS-Chem simulations show results consistent with the differences between emission inventories described in Section 3: simulated CO is lowest with FINN1.5 followed by GFED4s and then QFED2.4. This means that at sites where the model is biased high, the mean bias is smallest for GEOS-Chem/FINN1.5 and largest for GEOS-Chem/QFED2.4, while at sites where the model is biased low, the opposite is true. We note that there is evidence the TCCON retrievals may be biased high by 7% (Zhou et al., 2019). If this is the case, the GEOS-Chem high bias would more or less disappear for the FINN1.5 and GFED4s simulations and would be reduced to just under 10% for the QFED simulation.

When compared to the Darwin surface in situ measurements, the difference between the two models (GEOS-Chem and ACCESS-UKCA) with the same inventory (GFED4s) is striking: while the GEOS-Chem/GFED4s simulation underestimates observed CO by more than 30%, the ACCESS-UKCA/GFED4s simulation is within 2% of the observed mean. The reason for this difference will be explored in detail below. For the other measurements, the differences between models (ACCESS-UKCA/GFED4s vs. GEOS-Chem/GFED4s) is smaller than the difference between inventories when using the same model (GEOS-Chem).

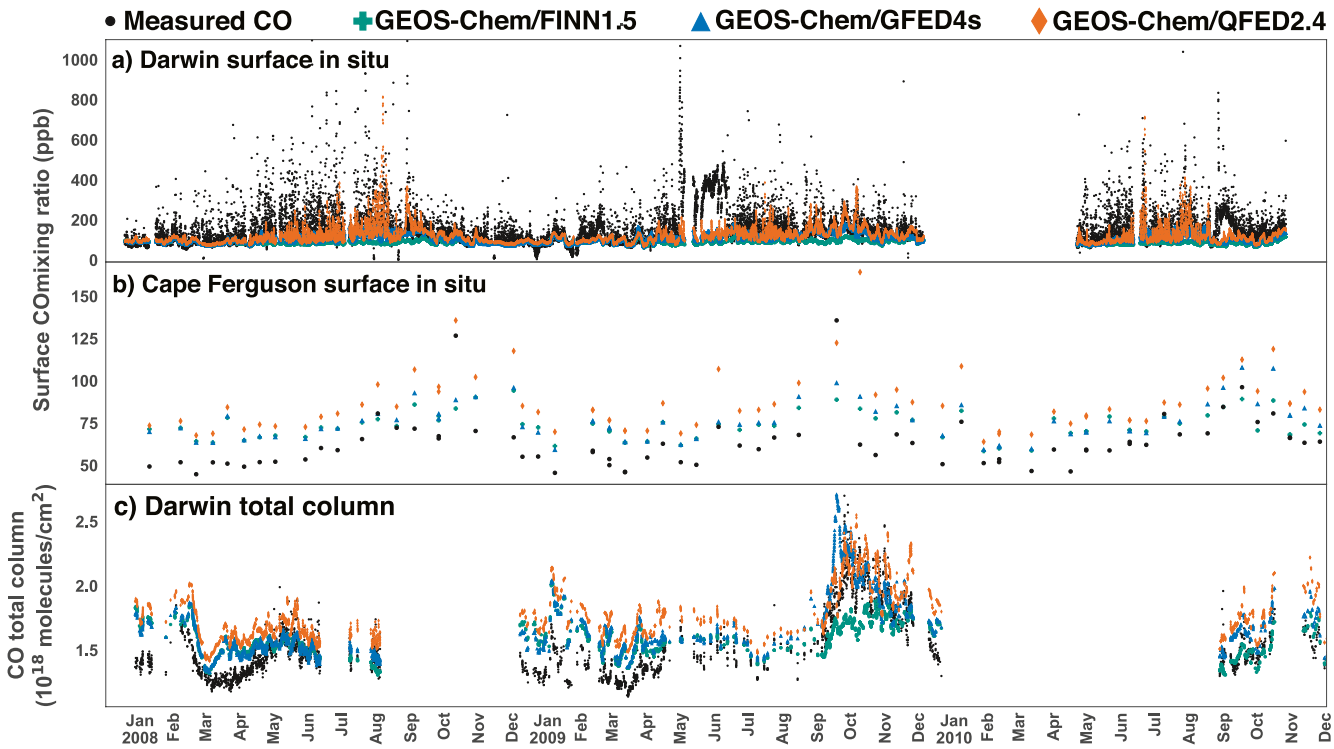

Figure 5. Time series of hourly measured (black) and simulated (colors) (a and b) surface and (c) total column CO in northern Australia. Note that ACCESS-UKCA output was not available at hourly resolution and is therefore not included in this figure. A similar figure averaged to monthly resolution can be found in the Supporting Information.

The mean biases tell us little about the relative suitability of each inventory to reproduce true Australian CO. For most of the year, Australian CO burdens are dominated by secondary production from oxidation of methane and other volatile organic compounds (Fisher et al., 2017). While some of these source compounds are associated with biomass burning, most are from biogenic emissions (Zeng et al., 2015). As a result, the overall mean CO values in the models are largely driven by sources other than biomass burning. Considering the documented general high CO bias in model simulations (Naik et al., 2013), a lower bias caused by a change in fire emission inventory might actually reflect a compensating effect of insufficient emissions. Therefore, mean biases are not an adequate test of inventory performance for biomass burning episodes.

Model variability, on the other hand, is more significantly influenced by biomass burning emissions due to the seasonal and episodic nature of this source (Edwards et al., 2006). GEOS-Chem tagged CO simulations from Fisher et al. (2017) (available only for 2009–2010) confirm these assumptions hold at the observation sites used here: secondary CO is responsible for 70%–90% of simulated CO throughout the year, while primary biomass burning emissions drive the annual cycle and interannual variability (see Figures S1–S3 in Supporting Information S1).

We therefore focus our analysis on model ability to reproduce variability rather than mean values. The relative ability of each simulation to reproduce the observed variability is quantified using the correlation coefficient r between each simulation and the measurements. Correlation coefficients calculated using both the hourly data (where available) and the monthly means are provided in Table 4. Model ability to reproduce observed variability at monthly timescales is also shown qualitatively in Figure 6, which compares the measured monthly mean CO to the simulated monthly mean after removing the mean bias. An equivalent figure without the mean bias subtracted can be found in the Supporting Information (Figure S4 in Supporting Information S1).

At Darwin, the GEOS-Chem simulations show limited ability to reproduce the observed variability from the surface in situ record. For the hourly observations, the correlation coefficients are $r = 0.25$ for GEOS-Chem/QFED2.4 and $r = 0.22$ for GEOS-Chem/GFED4s, implying the model captures at most ~6% of the observed variability (defined as r^2). Based on the temporal resolution of the emissions, we would expect better correlation with

Table 4
Correlation Coefficients (r) Between the Modeled and Measured Surface CO Mixing Ratios and Total Columns in Northern Australia[a]

	GEOS-Chem			ACCESS-UKCA[b]
	FINN1.5	QFED2.4	GFED4s	GFED4s
Surface in situ				
Darwin				
Hourly data	<0.01	0.25	0.22	
Monthly mean	−0.09	0.44	0.53	0.80
Cape Ferguson				
Hourly data	0.67	0.70	0.73	
Monthly mean	0.62	0.79	0.76	0.31
Total Column				
Darwin				
Hourly data	0.56	0.80	0.82	
Monthly mean	0.50	0.80	0.86	0.77
MOPITT[c]				
Monthly mean	0.80	0.94	0.91	0.70

[a]See Figure 1 for locations. [b]Only monthly mean model output is available for ACCESS-UKCA. [c]Averaged over the full northern Australia region shown in Figure 1.

the hourly data from the GFED4s simulation (3-hourly fire emissions) than the QFED2.4 simulation (daily fire emissions). Table 4 shows that this is not the case, implying the diurnal profile of the emissions is not the primary determinant of model ability to reproduce hourly variability at the Darwin surface site. At this temporal scale, small model-observation differences in meteorological parameters (e.g., wind speed and direction, boundary layer height) can significantly degrade model ability to match observed variability at the surface. For these simulations (GFED4s and QFED2.4), the correlation coefficients improve when both observation and model are averaged to monthly resolution, reproducing about 20% (QFED2.4) to 30% (GFED4s) of the observed monthly variability. This improvement shows that GEOS-Chem is better able to simulate the mean annual cycle than the individual events sampled in the hourly data, consistent with prior work (e.g., Lutsch et al., 2020; Zhang et al., 2014). With FINN1.5, the GEOS-Chem simulation is uncorrelated with the hourly data and weakly anti-correlated with the monthly mean data, suggesting major deficiencies in the ability of FINN1.5 to estimate either the magnitude or variability of fire emissions near Darwin.

ACCESS-UKCA performs significantly better for Darwin surface CO than all GEOS-Chem simulations, including when both models are driven by GFED4s emissions, with ACCESS-UKCA able to reproduce more than twice as much of the seasonal variability as GEOS-Chem/GFED4s. Figure 6 shows a much larger seasonal enhancement simulated by ACCESS-UKCA than by GEOS-Chem, particularly in 2009. The more accurate simulation of the seasonal peak by ACCESS-UKCA also explains the much smaller bias in ACCESS-UKCA relative to GEOS-Chem noted earlier (Table 3).

The large discrepancy between ACCESS-UKCA/GFED4s and GEOS-Chem/GFED4s is surprising given that we expect most of the CO seasonality at Darwin to be driven by biomass burning emissions (Edwards et al., 2006; Paton-Walsh et al., 2010), and both simulations use the same emission inventory. Other differences between the models that could influence simulation of the surface CO mixing ratio include horizontal resolution, land fraction (emittable area) in the grid cell containing Darwin, vertical injection height, and differences in meteorological fields caused by the use of different reanalysis products. We test the influence of each of these on simulated CO using the existing model output. We find that nearly all of the difference can be explained by differences in horizontal resolution between the models, as shown in Figure 7. Re-mapping the ACCESS-UKCA output from the native 1.25° × 1.875° resolution to the coarser 2° × 2.5° GEOS-Chem resolution substantially reduces the peak simulated CO as the emissions are diluted over the larger area, effectively eliminating the difference between the two models. Meanwhile, as shown in the Supporting Information (Figures S5 and S6 in Supporting Information S1), there appears to be little impact from the land versus ocean fraction in the Darwin grid cell (tested by sampling GEOS-Chem using grid cells with higher land fraction to the south and east) or from emission injection height and mixing (tested by comparing the simulated vertical distribution between models). These results highlight the strong horizontal resolution dependence of near-source observation-model comparisons and suggest a more robust test of the inventories at Darwin would require running a high-resolution model forced by the different inventories.

The Cape Ferguson surface in situ site is located substantially further from local emissions. As a result, the differences in model resolution are less important here. All simulations appear to have a 1-month lag in the timing of peak CO in 2008 and 2010 (Figure 6), which is a few months later at Cape Ferguson than at Darwin. However, missing data in 2009 and a generally sparse observation record due to the infrequent sampling (Figure 5) make it difficult to reliably determine the timing of the seasonal peak. ACCESS-UKCA performs notably worse ($r = 0.31$) than any of the GEOS-Chem simulations ($r = 0.62$–0.79) in simulating the annual cycle at Cape Ferguson. Amongst the GEOS-Chem simulations, the model best simulates the observed monthly means when using GFED4s and QFED2.4, reproducing 58% and 62% of the variability, respectively. With the mean biases removed, the GEOS-Chem/FINN1.5 simulation is nearly identical to GEOS-Chem/GFED4s for most of the simulation

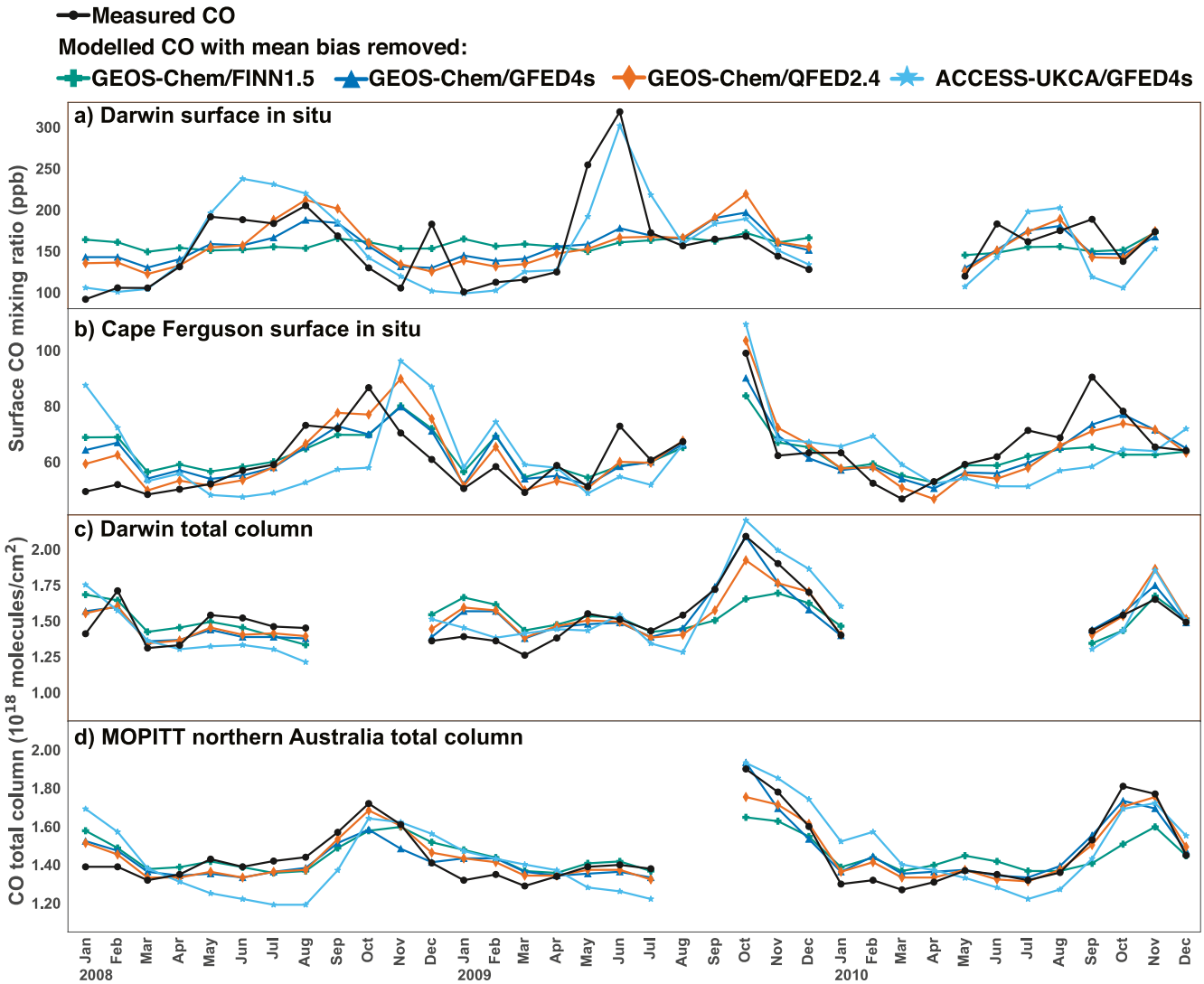

Figure 6. Monthly averaged (a and b) surface CO mixing ratio and (c and d) total column CO in northern Australia from measurements (black) and simulations (colors). The mean bias of each simulation has been removed to better highlight differences in variability.

period but misses the seasonal increase in the latter half of 2010 (Figure S4 in Supporting Information S1), reducing the correlation with the observations.

The total column observations are much less sensitive to nearby emissions than the surface measurements, as discussed previously. At Darwin, all simulations except GEOS-Chem/FINN1.5 are able to reproduce the majority of the variability observed in both the hourly data and the monthly means, with correlation coefficients of $r = 0.77$–0.86. All four simulations reproduce to some extent the peak total column CO observed in 2009, which occurs a few months later in the total column (October) than at the surface (June). However, the simulated peak is much smaller in the GEOS-Chem/FINN1.5 simulation than in the other simulations or the observations, leading to a weaker correlation. Although the GEOS-Chem CO total columns at Darwin are typically lower with GFED4s than QFED2.4, the situation is reversed during the 2009 peak (Figure S4 in Supporting Information S1). The 2009 enhancement in GFED4s is presumably due to the much larger emissions from the 2009 Indonesian fires in GFED4s than in the other inventories (Figure 4), coupled with meteorological conditions that favor transport from Indonesia to Darwin at this time of year (Figure S10 in Supporting Information S1). Overall, the GEOS-Chem/GFED4s simulation outperforms both the GEOS-Chem/QFED2.4 and the ACCESS-UKCA/GFED4s simulation in terms of both mean bias (Table 3) and correlation (Table 4).

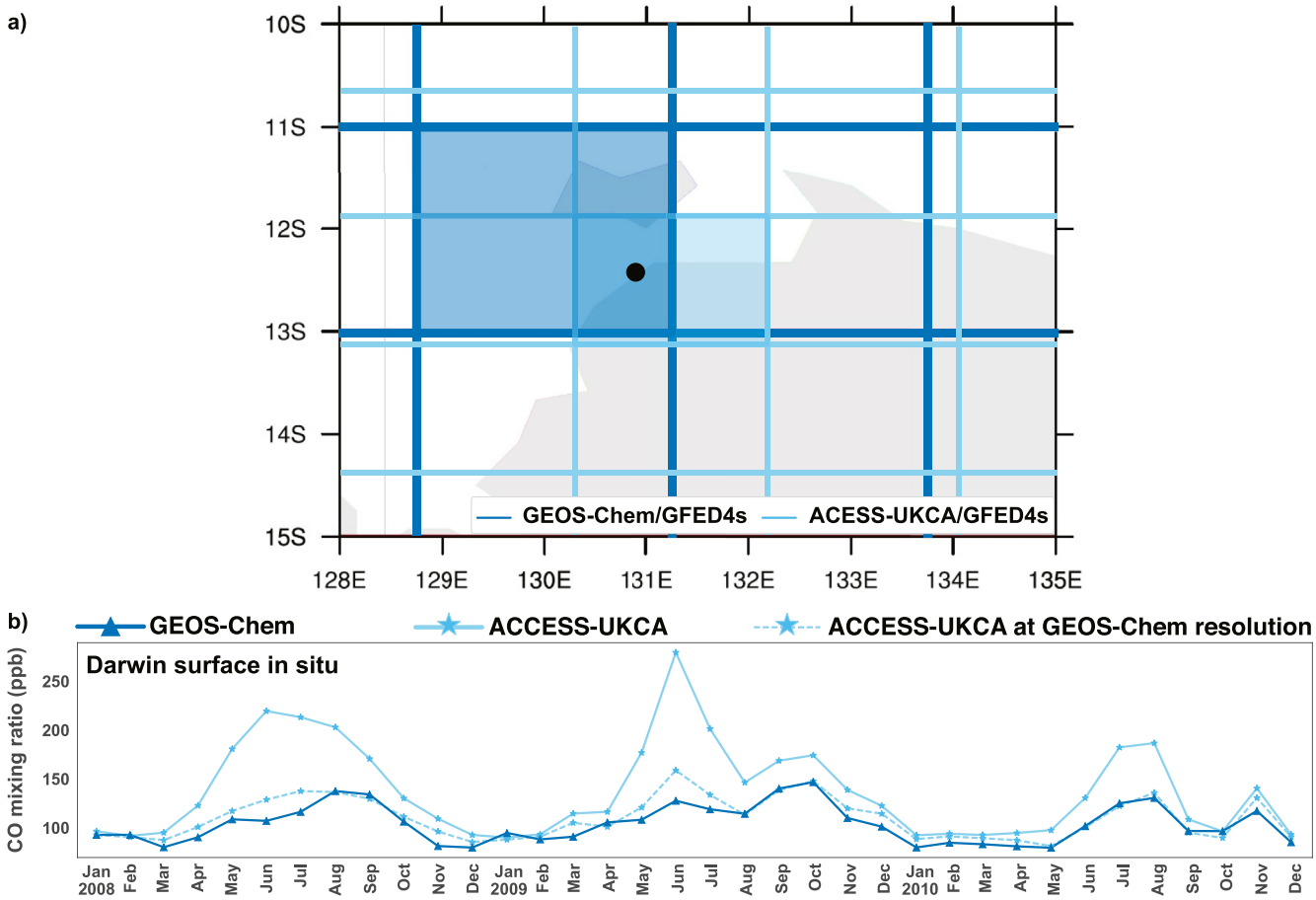

Figure 7. (a) GEOS-Chem (dark blue) and ACCESS-UKCA (light blue) model grid box locations in the region near Darwin. The black circle indicates the Darwin measurement site and the shaded boxes show the grid cells sampled in each model to represent Darwin. (b) Time series of modeled CO in Darwin surface air from GEOS-Chem (solid dark blue), ACCESS-UKCA (solid light blue), and ACCESS-UKCA re-mapped to the GEOS-Chem resolution (dashed light blue) using the Climate Data Operators first-order conservative remapping function (remapcon).

Comparison to the MOPITT satellite total columns averaged over northern Australia captures the seasonal cycle, but shows high bias in all simulations (Table 3), particularly from January to April (Figure S4 in Supporting Information S1). Consistent with the other comparisons, GEOS-Chem/FINN1.5 underestimates the seasonal CO peak. As seen previously for the Darwin total column data, GEOS-Chem/GFED4s provides the best simulation of the MOPITT data when considering both the mean bias (Table 3) and the correlation (Table 4), with this simulation able to reproduce 88% of the observed seasonal variability. Meanwhile, ACCESS-UKCA/GFED4s overestimates the strength of the seasonal cycle (Figure 6), degrading the correlation (Table 4).

4.2. Southern Australia

We perform a similar analysis using the datasets from southern Australia (Cape Grim surface in situ and Wollongong total column, plus MOPITT regional averages). Inventory analysis using these measurements comes with several caveats outlined here. Cape Grim is a remote site on the north-west coast of Tasmania, designed to primarily sample baseline or background air from the Southern Ocean region (Law et al., 2010; Loh et al., 2015). Therefore, differences at Cape Grim between the three GEOS-Chem simulations driven by the different inventories are generally more indicative of transported emissions from Africa and South America than local emissions from southern Australia. Meanwhile, Wollongong is a semi-urban site located on the east coast of New South Wales roughly 100 km south of Sydney. The site does occasionally sample smoke from local fires (e.g., Rea et al., 2016) but is also sensitive to anthropogenic, biogenic, and long-range transported biomass burning sources (Buchholz et al., 2016; Fisher et al., 2017; Lieschke et al., 2019).

Table 5
Mean Bias Between the Modeled and Measured Surface CO Mixing Ratios and Total Columns in Southern Australia[a]

	GEOS-Chem			ACCESS-UKCA[b]
	FINN1.5	QFED2.4	GFED4s	GFED4s
Surface in situ (ppbv)				
Cape Grim (observed mean = 55.8)				
Hourly data	18.3 (33%)	26.3 (47%)	18.6 (33%)	
Monthly mean	18.2 (33%)	26.2 (47%)	18.6 (33%)	12.0 (22%)
Total Column (10^{18} molec cm^{-2})				
Wollongong (observed mean = 1.36)				
Hourly data	0.128 (9%)	0.307 (23%)	0.159 (12%)	
Monthly mean	0.134 (10%)	0.314 (23%)	0.164 (12%)	0.025 (2%)
MOPITT[c] (observed mean = 1.35)				
Monthly mean	0.068 (5%)	0.207 (15%)	0.093 (7%)	0.006 (<1%)

[a]See Figure 1 for locations. [b]Only monthly mean model output is available for ACCESS-UKCA. [c]Averaged over the full southern Australia region shown in Figure 1.

The mean biases of each simulation relative to the Cape Grim and Wollongong measurements and the MOPITT satellite data (averaged over southern Australia) are shown in Table 5. Consistent with the results for the remote sites in northern Australia, all simulations show a high bias relative to the observations. As before, amongst the GEOS-Chem simulations, the magnitude of the bias correlates with the magnitude of the emissions, with the largest biases using QFED2.4 and the smallest using FINN1.5. Comparison to the hourly observations (Figure 8) shows that GEOS-Chem clearly overestimates the background CO amounts, irrespective of the emission inventory. Comparing the monthly means (shown in Figure S7 in Supporting Information S1) suggests ACCESS-UKCA provides a better simulation of the southern mid-latitude background than GEOS-Chem, with a smaller mean bias at Cape Grim and almost no bias at Wollongong (Table 5). As discussed previously, biases in the simulations reflect a combination of bias in the model background and inventory-driven differences; we therefore again focus on simulated variability (as represented by the correlation coefficient, *r*) to better differentiate the impacts of the different inventories.

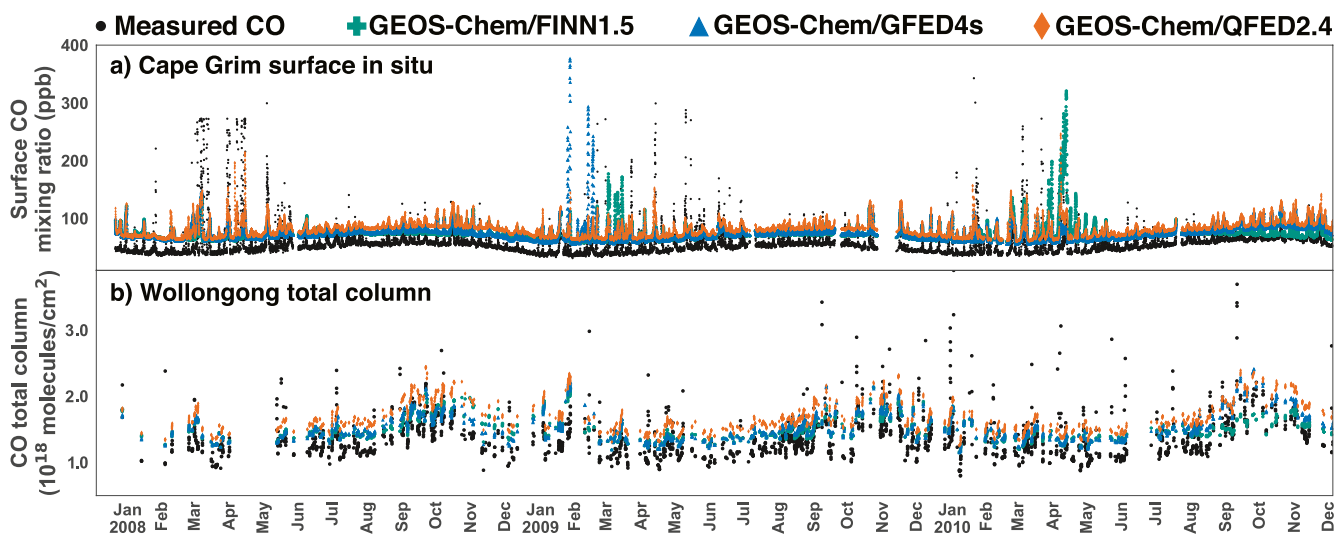

Figure 8. Time series of hourly measured (black) and simulated (colors) (a) surface and (b) total column CO in southern Australia. Note that ACCESS-UKCA output was not available at hourly resolution and is therefore not included in this figure. A similar figure averaged to monthly resolution can be found in Figure S7 in Supporting Information S1.

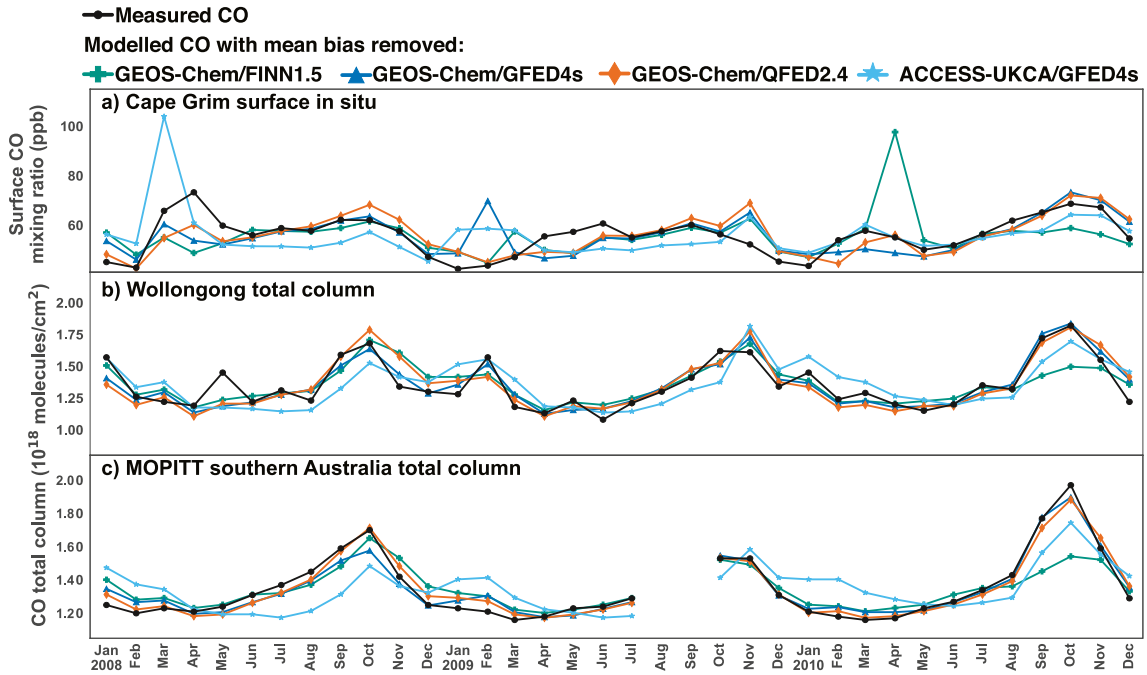

Figure 9. Monthly averaged (a) surface CO mixing ratio and (b and c) total column CO in southern Australia from measurements (black) and simulated (colors). The mean bias of each simulation has been removed to better highlight differences in variability.

Comparison of the observed and simulated variability (after subtracting the model mean biases) is shown in Figure 9. In the observational record, the only clear signal of the February 2009 Black Saturday event is seen in the Wollongong total columns. All four simulations capture this event to some extent, although only GEOS-Chem/GFED4s accurately simulates the strength of the enhancement (consistent with the emissions comparisons shown in Figure 3). In the models, the February 2009 event is also seen at Cape Grim by the two simulations that use the GFED4s emissions, but there is no equivalent enhancement in the observations or the other simulations. The fact that the anomalous enhancement is simulated by both models but only when using GFED4s implies it is caused by the strength of the emissions in GFED4s rather than by anomalous transport to the Cape Grim site. It is possible that the GFED4s inventory overestimates the emissions associated with the Black Saturday event, causing the February 2009 bias at Cape Grim. The more accurate simulation of the event at Wollongong could reflect compensating biases from emissions overestimates and plume dilution at the coarse model resolution (Eastham & Jacob, 2017; Rastigejev et al., 2010), given the significant distance from the fires to the Wollongong site. It should also be noted that while there has been recent progress in modeling smoke plume injection height (as reviewed by Paugam et al., 2016), both models used in this study inject all fire emissions at ground level, adding further uncertainty to plume dispersion. While Rea et al. (2016) found (using a different model) that CO from fires in southeast Australia was better reproduced when emissions were injected near the surface than distributed throughout the planetary boundary layer, these findings may not hold for the extreme conditions associated with the Black Saturday event (Field et al., 2016). Newer versions of GEOS-Chem allow smoke injection through multiple vertical layers, and use of this capability is a priority for future work.

Other observed variations can also be seen in the Cape Grim record in Figure 9, including an enhancement in surface CO in March–April 2008. The event is visible in all simulations and in the observations, although the FINN1.5 and GFED4s simulations underestimate the duration and ACCESS-UKCA greatly overestimates the magnitude. The March–April 2008 enhancement is likely due to a large fire in the Tarkine Wilderness, which burned nearly 20,000 ha in northwest Tasmania near the Cape Grim site (BrisbaneTimes, 2008). The much larger enhancement in the ACCESS-UKCA/GFED4s simulation than in the equivalent GEOS-Chem/GFED4s simulation likely reflects the same resolution dependence seen for the local fires at Darwin; however, in this case GFED4s appears to overestimate the emissions leading to the high bias in the better resolved ACCESS-UKCA simulation. The GEOS-Chem/FINN1.5 simulation at Cape Grim shows a similarly large enhancement in April 2010 that is not seen in the observations or the other simulations. The magnitude of the peak again suggests local

Table 6
Correlation Coefficients (r) Between the Modeled and Measured Surface CO Mixing Ratios and Total Columns in Southern Australia[a]

	GEOS-Chem			ACCESS-UKCA[b]
	FINN1.5	QFED2.4	GFED4s	GFED4s
Surface in situ				
Cape Grim				
Hourly data	0.39	0.66	0.48	
Monthly mean	0.22	0.72	0.51	0.35
Total column				
Wollongong				
Hourly data	0.58	0.65	0.66	
Monthly mean	0.78	0.86	0.90	0.70
MOPITT[c]				
Monthly mean	0.86	0.98	0.97	0.64

[a]See Figure 1 for locations. [b]Only monthly mean model output is available for ACCESS-UKCA. [c]Averaged over the full southern Australia region shown in Figure 1.

emissions; however, in this case there is no evidence of nearby fires and the enhancement appears to be the consequence of erroneous emissions in the FINN1.5 inventory, consistent with the emissions shown in Figure 3.

Overall, GEOS-Chem driven by QFED2.4 provides the best simulation of the observed variability at Cape Grim, with a correlation coefficient of $r \approx 0.7$ (compared to 0.2–0.5 for the other simulations), as shown in Table 6. At Wollongong, there is less difference between simulations in terms of ability to reproduce observed variability. GEOS-Chem simulations driven by QFED2.4 and GFED4s perform similarly to one another, with correlation coefficients of 0.65-0.66 against the observed hourly data and 0.86-0.90 against the observed monthly means. Figure 9 shows that the monthly variability simulated by GEOS-Chem/FINN1.5 is nearly identical to that from the other GEOS-Chem simulations, except in late 2010 when GEOS-Chem/FINN1.5 underestimates the seasonal peak (leading to the weaker correlation in Table 6). The source attribution in the Supporting Information (Figure S2 in Supporting Information S1) suggests this peak is associated with the South American fires, implying FINN1.5 underestimates emissions from these fires (as discussed previously in Section 3). Despite having the lowest bias (Table 5), the ACCESS-UKCA simulation is the least correlated with the Wollongong observations ($r = 0.70$) but still captures roughly half of the observed monthly variability.

The MOPITT data for southern Australia provide little additional insight. As at Wollongong, the GEOS-Chem simulations driven by GFED4s and QFED2.4 provide the best simulation of the annual cycle. As the MOPITT data have been averaged over the entire southern Australia region, they primarily reflect the southern mid-latitude CO background with little influence from primary biomass burning emissions (Figure S3 in Supporting Information S1). The exception is the influence of the South American fires in late 2010, when the FINN1.5 underestimate is again evident. As at Wollongong, ACCESS-UKCA provides the poorest simulation of the annual cycle, with model overestimates in the first half of the year and underestimates in the second half that are not seen in the GEOS-Chem simulations. A similar pattern was seen in the ACCESS-UKCA comparison to MOPITT in northern Australia (Figure 6) and is almost certainly due to model chemistry (secondary CO production and/or loss) rather than any direct impact of the biomass burning emissions.

4.3. Statistical Summary and Recommendations

Figure 10 summarizes the simulation-measurement comparisons using a Taylor diagram to simultaneously compare the different simulations on the basis of their correlation coefficients, root mean squared error (RMSE) and standard deviation relative to the observations. The RMSE values are calculated after removing the mean bias. The standard deviations are normalized to the relevant observational dataset such that values greater than 1 represent greater variability in the simulations than was observed. The Taylor diagram provides a condensed visual representation of the overall capabilities of the four simulations. An ideal simulation would have an RMSE of 0.0, normalized standard deviation of 1.0, and correlation coefficient of 1.0, indicated on the figure as the black circle labeled "obs." The closer each point sits to the "obs" marker, the better that simulation represents the observations. We use the monthly mean data here to enable comparison between GEOS-Chem and ACCESS-UKCA simulations on equal footing.

Consistent with the results presented previously, the models perform best when compared to the regionally averaged satellite observations followed by the ground-based total column observations, with the worst performance relative to the surface in situ measurements. This summary reinforces the point that the coarse resolution models used here are best suited to interpretation of measurements that represent large spatial scales. Higher resolution models would be required to more accurately resolve and evaluate emissions at the local scale measured by the surface in situ data.

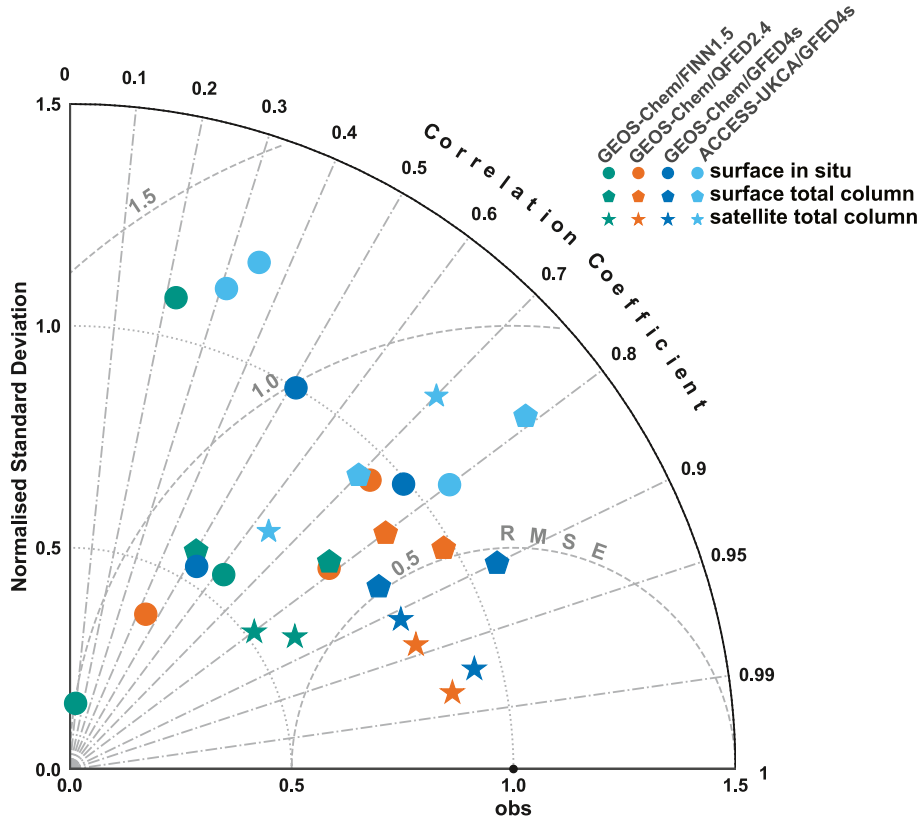

Figure 10. Taylor diagram summarizing the evaluation of the four simulations against monthly mean surface in-situ (circles), surface total column (hexagons), and regional average MOPITT satellite (stars) measurements. Evaluation metrics include the normalized standard deviation (radial coordinate, normalized to the observed standard deviation), correlation coefficient (angular coordinate), and root mean square error (dashed semi-circles). The black dot labeled "obs" denotes the ideal performance (identical to the observations).

More importantly, Figure 10 shows that the Australian observational record is most accurately simulated using GEOS-Chem with either GFED4s or QFED2.4 emissions. Our results suggest that the ACCESS-UKCA simulation, which currently uses only GFED4s emissions, would not be improved by using the FINN1.5 or QFED2.4 emissions. Instead, the poorer performance by ACCESS-UKCA than GEOS-Chem/GFED4s (except at the Darwin surface) may be partly explained by the fact that the ACCESS-UKCA chemistry scheme has some limitations compared to GEOS-Chem—for example, ACCESS-UKCA lumps ethane, ethene, and ethyne into ethane and lumps propene into propane; a generic "NMVOC" (non-methane volatile organic compound) species is used as proxy for acetaldehyde, and ketone is used as proxy for acetone. These simplifications in organic compounds will impact CO through secondary production, both in biomass burning plumes and in background air.

Comparison of the three GEOS-Chem simulations suggests that FINN1.5 is not fit-for-purpose in simulating CO over Australia. Both near-source and downwind observations in northern Australia imply large errors in FINN1.5 estimates of emissions from savanna fires, which are virtually non-existent relative to the other inventories (Figure 3). Meanwhile, observations in southern Australia that largely capture the influence of transported emissions also suggest that FINN1.5 underestimates CO biomass burning emissions in South America. Liu et al. (2020) previously found that simulations driven by FINN1.5 also performed poorly relative to other inventories in Indonesia. While their results were based on fine particulate matter, we expect similar biases would affect simulation of Indonesian CO emissions, with likely implications for CO transported to northern Australia. Given the biases in both Australian and Indonesian emissions, we therefore recommend that FINN1.5 not be used for Australian modeling studies. The results from this study have motivated in part updates to the next version of FINN (version 2, in preparation) and future evaluation is recommended when that version is released.

5. Conclusions

Emissions from Australian biomass burning are a primary driver of seasonal and interannual variability in Australian atmospheric composition but remain highly uncertain due to a dearth of measurements in the unique Australian environment. In this work, we used surface in situ, ground-based total column, and satellite total column observations to evaluate the ability of two global atmospheric chemistry models (GEOS-Chem and ACCESS-UKCA) and three global biomass burning emission inventories (FINN1.5, GFED4s, and QFED2.4) to simulate CO in the Australian atmosphere from 2008 to 2010.

Comparison of CO emissions from the three inventories showed that FINN1.5 estimates substantially lower emissions than the other two inventories, particularly in the northern Australia savanna. Estimates from GFED4s and QFED2.4 are similar in seasonality to one another but with higher magnitude in QFED2.4. On a hemispheric scale, the Australian emissions are dwarfed by emissions from Africa and South America, with Australia responsible for 1%–15% of total Southern Hemisphere fire emissions, complicating the interpretation of the Australian evaluation.

Of the existing observational datasets, we found that only the Darwin surface in situ record provides information on fresh biomass burning emissions from Australian savanna fires. Here, GEOS-Chem significantly underestimated the CO surface mixing ratios and reproduced little of the observed variability on either hourly or monthly timescales, irrespective of the biomass burning inventory used. ACCESS-UKCA, on the other hand, simulated Darwin surface CO to within 2% of the observed mean and reproduced nearly two-thirds of the observed seasonal variability, with the difference between the two models attributable to the finer horizontal resolution of ACCESS-UKCA. This resolution dependence implies that a more robust test of the inventories at Darwin would require use of a finer resolution model.

Elsewhere, the existing measurements in both northern and southern Australia are primarily sensitive to background CO and aged smoke. The simulations overestimated the CO background at these sites (with the exception of ACCESS-UKCA at Wollongong), hindering evaluation of the biomass burning inventories. Although the inventories differed substantially in terms of the magnitude of Australian emissions (Section 3), the relative impacts of the bias in background CO versus the bias in Australian biomass burning CO could not be disentangled.

Evaluation therefore focused on the ability of each simulation to reproduce the observed variability. Comparing the two models driven by the same inventory (GFED4s), GEOS-Chem captured more of the observed variability at the remote sites than ACCESS-UKCA, perhaps due to the more complex chemical mechanism (which would influence the secondary production and loss of CO). Amongst the three GEOS-Chem simulations, GFED4s and QFED2.4 performed similarly. The simulation with FINN1.5 was notably worse, particularly at Darwin where almost no seasonal variability was simulated, highlighting insufficient emissions from savanna fires in FINN1.5. Only GFED4s captured the enhanced CO at Wollongong from the Black Saturday event; however, the GFED4s simulations overestimated CO at Cape Grim during this event, implying the emissions associated with the event may be overestimated in GFED4s. Overall, we recommend that global CO modeling studies with focus on Australia and/or the Southern Hemisphere use GFED4s emissions rather than QFED2.4 (which leads to large biases when coupled with the existing biases in the CO background) or FINN1.5 (which underestimates observed variability).

Our results also showed that existing observations in Australia can only partially constrain global model estimates of biomass burning. Only the Darwin surface in situ measurements are sensitive to fresh fire emissions, but simulation of CO from these emissions is highly sensitive to model resolution. Meanwhile, the total column CO measurements at Darwin and Wollongong are less sensitive to resolution and boundary layer effects but are significantly impacted by transported smoke from large emissions upwind in Africa and South America. Preliminary evaluation using shorter-lived formaldehyde at Wollongong provided no additional insight, as there was virtually no difference between formaldehyde simulated at Wollongong using the three different inventories (not shown here). While formaldehyde has not previously been measured systematically at Darwin, recent equipment upgrades will provide a formaldehyde total column record in future, which we expect to provide more useful constraints on biomass burning emissions from Australian savanna fires.

Australian fires are a key contributor to global carbon emissions (Prosperi et al., 2020; Shi et al., 2015; van der Werf et al., 2017) and to Australia's carbon budget (Haverd et al., 2013, 2015). Climate change is increasing the

risk of extreme fire seasons in Australia (van Oldenborgh et al., 2021), with potentially significant augmentation of carbon emissions as seen during the recent 2019–2020 megafires (Shiraishi & Hirata, 2021). At the same time, more frequent fires may be reducing the carbon stores and associated fire emissions from Australia's southeastern forests (Bowman et al., 2020), and adoption of Aboriginal fire management practices are already decreasing fire frequency and potentially emissions from the northern savannas (Ansell et al., 2020; Liu et al., 2021). Implementing these ongoing environmental and management changes into the next generation of global biomass burning emission inventories is a key priority for accurately simulating Australian fire emissions and their regional and global impacts.

Acronyms

ACCESS-UKCA	Australian community climate and earth system simulator - United Kingdom chemistry and aerosol
ECMWF	European centre for medium-range weather forecasts
FINN1.5	Fire INventory from NCAR version 1.5
GEOS	Goddard earth observing system
GFED4s	Global fire emissions dataset version 4s
MODIS	Moderate resolution imaging spectroradiometer
MOPITT	Measurements of pollution in the troposphere
QFED2.4	Quick fire emissions dataset version 2.4

Data Availability Statement

In situ CO data at Darwin are available from the corresponding author by request. In situ data for Cape Grim were provided by Dr. P Krummel of CSIRO's Climate Science Centre and are available upon request. In situ data at Cape Ferguson were downloaded from the World Data Centre for Greenhouse Gases webpage (https://gaw.kishou.go.jp/search/station#CFA). Ground-based total column at Wollongong were downloaded from the NDACC network database (https://ftp.cpc.ncep.noaa.gov/ndacc/station/wollong/) and funded through ARC grant LE0668470. Ground-based total column data at Darwin were downloaded from the TCCON network database (https://data.caltech.edu/records/291) and funded through several ARC grants (DP140101552, DP160101598, DP110103118, DP0879468) and NASA grants (NAG5-12 247, NNG05-GD07 G). MOPITT Version 7 level 3 data were obtained from the NASA data archive (https://l5eil01.larc.nasa.gov:22000/distribution/pub/MOPITT/MOP03JM.007/). Information to download, install and run GEOS-Chem is available from the GEOS-Chem wiki page http://wiki.seas.harvard.edu/geos-chem/index.php/Main_Page. Set-up files for this study and analysis codes (python) of the output files are available in Github and archived in Zenodo: https://zenodo.org/badge/latestdoi/380869004.

Acknowledgments
We gratefully acknowledge Clare Paton-Walsh for helpful comments on the manuscript. This work was funded in part by ARC Discovery Project DP160101598 and was undertaken with the assistance of resources provided at the National Computational Infrastructure (NCI) National Facility systems at the Australian National University through the National Computational Merit Allocation Scheme (project m19) supported by the Australian Government. The ACCESS model development was supported by funding from the Australian Climate Change Science Programme (ACCSP) and the model simulations were made with the assistance of resources and services from the NCI, which is supported by the Australian government. Martin Dix and Scott Wales are acknowledged for their help with the ACCESS model setup. The NCAR MOPITT project is supported by the NASA Earth Observing System (EOS) Program. Dr Maximilien Desservettaz was supported during this work by a CSIRO Office of the Chief Executive Postgraduate Scholarship. NMD is supported by an ARC Future Fellowship, FT180100327. CSIRO is thanked for the long-term support of the CSIRO GASLAB flask network, including Cape Ferguson. The Cape Grim in situ CO measurements are supported by the Australian Bureau of Meteorology, CSIRO, and the National Aeronautics and Space Administration (Grant No. NNX16AC98G). Open access publishing facilitated by University of Wollongong, as part of the Wiley - University of Wollongong agreement via the Council of Australian University Librarians.

References

Abraham, N. L., Archibald, A. T., Bellouin, N., Boucher, O., Braesicke, P., Bushell, A., et al. (2012). *Unified model documentation paper no. 84: United Kingdom chemistry and aerosol (UKCA) technical description MetUM version 8.2*. UK Met Office.

Akagi, S. K., Yokelson, R. J., Wiedinmyer, C., Alvarado, M. J., Reid, J. S., Karl, T., et al. (2011). Emission factors for open and domestic biomass burning for use in atmospheric models. *Atmospheric Chemistry and Physics*, *11*(9), 4039–4072. https://doi.org/10.5194/acp-11-4039-2011

Andreae, M. O. (2019). Emission of trace gases and aerosols from biomass burning–an updated assessment. *Atmospheric Chemistry and Physics*, *19*(13), 8523–8546. https://doi.org/10.5194/acp-19-8523-2019

Andreae, M. O., & Merlet, P. (2001). Emission of trace gases and aerosols from biomass burning. *Global Biogeochemical Cycles*, *15*(4), 955–966. https://doi.org/10.1029/2000gb001382

Ansell, J., Evans, J., Rangers, A., Rangers, A. S., Rangers, D., Rangers, J., et al. (2020). Contemporary Aboriginal savanna burning projects in Arnhem Land: A regional description and analysis of the fire management aspirations of traditional owners. *International Journal of Wildland Fire*, *29*(5), 371. https://doi.org/10.1071/wf18152

Bey, I., Jacob, D. J., Yantosca, R. M., Logan, J. A., Field, B. D., Fiore, A. M., et al. (2001). Global modeling of tropospheric chemistry with assimilated meteorology: Model description and evaluation. *Journal of Geophysical Research: Atmospheres*, *106*(D19), 23073–23095. https://doi.org/10.1029/2001jd000807

Bi, D., Dix, M., Marsland, S., O'Farrell, S., Rashid, H., Uotila, P., et al. (2013). The ACCESS coupled model: Description, control climate and evaluation. *Australian Meteorological and Oceanographic Journal*, *63*(1), 41–64. https://doi.org/10.22499/2.6301.004

Bowman, D. M., Williamson, G. J., Price, O. F., Ndalila, M. N., & Bradstock, R. A. (2020). Australian forests megafires and the risk of dwindling carbon stocks. *Plant, Cell and Environment*, *44*(2), 347–355. https://doi.org/10.1111/pce.13916

BrisbaneTimes (2008). *Tassie fires 'can be seen from victoria'*. Retrieved from https://www.brisbanetimes.com.au/national/queensland/tassie-fires-can-be-seen-from-victoria-20080320-ge9s9n.html

Buchholz, R. R., Deeter, M. N., Worden, H. M., Gille, J., Edwards, D. P., Hannigan, J. W., et al. (2017). Validation of MOPITT carbon monoxide using ground-based Fourier transform infrared spectrometer data from NDACC. *Atmospheric Measurement Techniques*, *10*(5), 1927–1956. https://doi.org/10.5194/amt-10-1927-2017

Buchholz, R. R., Hammerling, D., Worden, H. M., Deeter, M. N., Emmons, L. K., Edwards, D. P., & Monks, S. A. (2018). Links between carbon monoxide and climate indices for the southern hemisphere and tropical fire regions. *Journal of Geophysical Research: Atmospheres*, *123*(17), 9786–9800. https://doi.org/10.1029/2018jd028438

Buchholz, R. R., Paton-Walsh, C., Griffith, D. W. T., Kubistin, D., Caldow, C., Fisher, J. A., et al. (2016). Source and meteorological influences on air quality (CO, CH_4 & CO_2) at a Southern Hemisphere urban site. *Atmospheric Environment*, *126*, 274–289. https://doi.org/10.1016/j.atmosenv.2015.11.041

Carter, T. S., Heald, C. L., Jimenez, J. L., Campuzano-Jost, P., Kondo, Y., Moteki, N., et al. (2020). How emissions uncertainty influences the distribution and radiative impacts of smoke from fires in North America. *Atmospheric Chemistry and Physics*, *20*(4), 2073–2097. https://doi.org/10.5194/acp-20-2073-2020

Cook, G., Hurst, D. F., & Griffith, D. W. (1995). Atmospheric trace gas emissions from tropical australian savanna fires. *CALMScience*, 123–128.

Cruz, M. G., Sullivan, A. L., Gould, J. S., Sims, N. C., Bannister, A. J., Hollis, J. J., & Hurley, R. J. (2012). Anatomy of a catastrophic wildfire: The Black Saturday Kilmore East fire in Victoria, Australia. *Forest Ecology and Management*, *284*, 269–285. https://doi.org/10.1016/j.foreco.2012.02.035

Darmenov, A., & da Silva, A. (2015). The Quick fire emissions dataset (QFED)–documentation of versions 2.1, 2.2 and 2.4. *NASA Technical Report Series on Global Modeling and Data Assimilation*, *38*, 199.

Dee, D. P., Uppala, S. M., Simmons, A., Berrisford, P., Poli, P., Kobayashi, S., et al. (2011). The ERA-Interim reanalysis: Configuration and performance of the data assimilation system. *Quarterly Journal of the Royal Meteorological Society*, *137*(656), 553–597. https://doi.org/10.1002/qj.828

Deeter, M. N., Edwards, D. P., Francis, G. L., Gille, J. C., Martínez-Alonso, S., Worden, H. M., & Sweeney, C. (2017). A climate-scale satellite record for carbon monoxide: The MOPITT version 7 product. *Atmospheric Measurement Techniques*, *10*(7), 2533–2555. https://doi.org/10.5194/amt-10-2533-2017

Desservettaz, M., Paton-Walsh, C., Griffith, D. W. T., Kettlewell, G., Keywood, M. D., Vanderschoot, M. V., et al. (2017). Emission factors of trace gases and particles from tropical savanna fires in Australia. *Journal of Geophysical Research: Atmospheres*, *122*, 6059–6074. https://doi.org/10.1002/2016JD025925

Deutscher, N. M., Griffith, D. W. T., Bryant, G. W., Wennberg, P. O., Toon, G. C., Washenfelder, R. A., et al. (2010). Total column CO_2 measurements at Darwin, Australia–site description and calibration against in situ aircraft profiles. *Atmospheric Measurement Techniques*, *3*(4), 947–958. https://doi.org/10.5194/amt-3-947-2010

Drummond, J. R., & Mand, G. S. (1996). The Measurements of Pollution in the Troposphere (MOPITT) instrument: Overall performance and calibration requirements. *Journal of Atmospheric and Oceanic Technology*, *13*(2), 314–320. https://doi.org/10.1175/1520-0426(1996)013<0314:tmopit>2.0.co;2

Eastham, S. D., & Jacob, D. J. (2017). Limits on the ability of global Eulerian models to resolve intercontinental transport of chemical plumes. *Atmospheric Chemistry and Physics*, *17*(4), 2543–2553. https://doi.org/10.5194/acp-17-2543-2017

Edwards, D. P., Emmons, L. K., Gille, J. C., Chu, A., Attié, J.-L., Giglio, L., et al. (2006). Satellite-observed pollution from Southern Hemisphere biomass burning. *Journal of Geophysical Research*, *111*(D14). https://doi.org/10.1029/2005jd006655

Emmons, L. K., Edwards, D. P., Deeter, M. N., Gille, J. C., Campos, T., Nédélec, P., et al. (2009). Measurements of pollution in the troposphere (MOPITT) validation through 2006. *Atmospheric Chemistry and Physics*, *9*(5), 1795–1803. https://doi.org/10.5194/acp-9-1795-2009

Eyring, V. (2005). Emissions from international shipping: 1. The last 50 years. *Journal of Geophysical Research*, *110*(D17). https://doi.org/10.1029/2004jd005619

Field, C. B., Randerson, J. T., & Malmström, C. M. (1995). Global net primary production: Combining ecology and remote sensing. *Remote Sensing of Environment*, *51*(1), 74–88. https://doi.org/10.1016/0034-4257(94)00066-v

Field, R. D., Luo, M., Fromm, M., Voulgarakis, A., Mangeon, S., & Worden, J. (2016). Simulating the Black Saturday 2009 smoke plume with an interactive composition-climate model: Sensitivity to emissions amount, timing, and injection height. *Journal of Geophysical Research: Atmospheres*, *121*(8), 4296–4316. https://doi.org/10.1002/2015jd024343

Fisher, J. A., Murray, L. T., Jones, D. B. A., & Deutscher, N. M. (2017). Improved method for linear carbon monoxide simulation and source attribution in atmospheric chemistry models illustrated using GEOS-Chem v9. *Geoscientific Model Development*, *10*(11), 4129–4144. https://doi.org/10.5194/gmd-10-4129-2017

Giglio, L., Randerson, J. T., & van der Werf, G. R. (2013). Analysis of daily, monthly, and annual burned area using the fourth-generation global fire emissions database (GFED4). *Journal of Geophysical Research: Biogeosciences*, *118*(1), 317–328. https://doi.org/10.1002/jgrg.20042

Gill, A. M. (1975). Fire and the Australian flora: A review. *Australian Forestry*, *38*(1), 4–25. https://doi.org/10.1080/00049158.1975.10675618

Griffith, D., Deutscher, N., Velazco, V., Wennberg, P., Yavin, Y., Keppel-Aleks, G., et al. (2014). *Tccon data from Darwin (au), release ggg2014* (Vol. 10). https://doi.org/10.14291/tccon.ggg2014.darwin01.R0/1149290

Griffith, D., Deutscher, N. M., Caldow, C., Kettlewell, G., Riggenbach, M., & Hammer, S. (2012). A Fourier transform infrared trace gas and isotope analyser for atmospheric applications. *Atmospheric Measurement Techniques*, *5*(10), 2481–2498. https://doi.org/10.5194/amt-5-2481-2012

Guenther, A. B., Jiang, X., Heald, C. L., Sakulyanontvittaya, T., Duhl, T., Emmons, L. K., & Wang, X. (2012). The model of emissions of gases and aerosols from nature version 2.1 (MEGAN2.1): An extended and updated framework for modeling biogenic emissions. *Geoscientific Model Development*, *5*(6), 1471–1492. https://doi.org/10.5194/gmd-5-1471-2012

Haverd, V., Raupach, M. R., Briggs, P. R., Davis, S. J., Law, R. M., Meyer, C. P., et al. (2013). The Australian terrestrial carbon budget. *Biogeosciences*, *10*(2), 851–869. https://doi.org/10.5194/bg-10-851-2013

Haverd, V., Raupach, M. R., Briggs, P. R., Canadell, J. G., Davis, S. J., Law, R. M., et al. (2015). Corrigendum to "The Australian Terrestrial Carbon Budget" published in Biogeosciences 10, 851–869, 2013. *Biogeosciences*, *12*(11), 3603–3605. https://doi.org/10.5194/bg-12-3603-2015

Hedelius, J. K., He, T.-L., Jones, D. B. A., Baier, B. C., Buchholz, R. R., De Mazière, M., et al. (2019). Evaluation of MOPITT version 7 joint TIR–NIR X_{CO} retrievals with TCCON. *Atmospheric Measurement Techniques*, *12*(10), 5547–5572. https://doi.org/10.5194/amt-12-5547-2019

Hoelzemann, J. J., Schultz, M. G., Brasseur, G. P., Granier, C., & Simon, M. (2004). Global Wildland Fire Emission Model (GWEM): Evaluating the use of global area burnt satellite data. *Journal of Geophysical Research*, *109*(D14). https://doi.org/10.1029/2003jd003666

Hurst, D. F., Griffith, D. W. T., Carras, J. N., Williams, D. J., & Fraser, P. J. (1994). Measurements of trace gases emitted by Australian savanna fires during the 1990 dry season. *Journal of Atmospheric Chemistry*, *18*(1), 33–56. https://doi.org/10.1007/bf00694373

Hurst, D. F., Griffith, D. W. T., & Cook, G. D. (1994). Trace gas emissions from biomass burning in tropical Australian savannas. *Journal of Geophysical Research*, *99*(D8), 16441–16456. https://doi.org/10.1029/94jd00670

Kaiser, J. W., Heil, A., Andreae, M. O., Benedetti, A., Chubarova, N., Jones, L., et al. (2012). Biomass burning emissions estimated with a global fire assimilation system based on observed fire radiative power. *Biogeosciences*, *9*(1), 527–554. https://doi.org/10.5194/bg-9-527-2012

Keppel-Aleks, G., Wennberg, P. O., Washenfelder, R. A., Wunch, D., Schneider, T., Toon, G. C., et al. (2012). The imprint of surface fluxes and transport on variations in total column carbon dioxide. *Biogeosciences*, *9*(3), 875–891. Retrieved from https://bg.copernicus.org/articles/9/875/2012/

Khalil, M., & Rasmussen, R. (1984). Carbon monoxide in the earth's atmosphere: Increasing trend. *Science*, *224*(4644), 54–56. https://doi.org/10.1126/science.224.4644.54

Krummel, P., Langenfelds, R., & Loh, Z. (2016). *Atmospheric CO at Cape Ferguson by Commonwealth Scientific and Industrial Research Organisation*. Dataset published as CO_CFA_surface-flask_CSIRO_data1 at WDCGG, ver. 2021-0408-1004. https://doi.org/10.50849/WDCGG_0016-5010-3001-01-02-9999

Lamarque, J.-F., Shindell, D. T., Josse, B., Young, P. J., Cionni, I., Eyring, V., et al. (2013). The atmospheric chemistry and climate model intercomparison project (ACCMIP): Overview and description of models, simulations and climate diagnostics. *Geoscientific Model Development*, *6*(1), 179–206. https://doi.org/10.5194/gmd-6-179-2013

Langenfelds, R. L., Francey, R. J., Pak, B. C., Steele, L. P., Lloyd, J., Trudinger, C. M., & Allison, C. E. (2002). Interannual growth rate variations of atmospheric CO_2 and its $\delta^{13}C$, H_2, CH_4, and CO between 1992 and 1999 linked to biomass burning. *Global Biogeochemical Cycles*, *16*(3), 21-1. https://doi.org/10.1029/2001gb001466

Law, R. M., Steele, L. P., Krummel, P. B., & Zahorowski, W. (2010). Synoptic variations in atmospheric co2 at cape grim: A model intercomparison. *Tellus B: Chemical and Physical Meteorology*, *62*(5), 810–820. https://doi.org/10.1111/j.1600-0889.2010.00470.x

Lewis, S. L., Brando, P. M., Phillips, O. L., van der Heijden, G. M. F., & Nepstad, D. (2011). The 2010 Amazon Drought. *Science*, *331*(6017), 554. https://doi.org/10.1126/science.1200807

Lieschke, K. J., Fisher, J. A., Paton-Walsh, C., Jones, N. B., Greenslade, J. W., Burden, S., & Griffith, D. W. T. (2019). Decreasing trend in formaldehyde detected from 20-year record at Wollongong Southeast Australia. *Geophysical Research Letters*, *46*(14), 8464–8473. https://doi.org/10.1029/2019gl083757

Liu, T., Mickley, L. J., Marlier, M. E., DeFries, R. S., Khan, M. F., Latif, M. T., & Karambelas, A. (2020). Diagnosing spatial biases and uncertainties in global fire emissions inventories: Indonesia as regional case study. *Remote Sensing of Environment*, *237*, 111557. https://doi.org/10.1016/j.rse.2019.111557

Liu, T., Mickley, L. J., & McCarty, J. L. (2021). Global search for temporal shifts in fire activity: Potential human influence on southwest Russia and north Australia fire seasons. *Environmental Research Letters*, *16*(4), 044023. https://doi.org/10.1088/1748-9326/abe328

Loh, Z., Law, R., Haynes, K., Krummel, P., Steele, L., Fraser, P., et al. (2015). Simulations of atmospheric methane for cape grim, Tasmania, to constrain Southeastern Australian methane emissions. *Atmospheric Chemistry and Physics*, *15*(1), 305–317. https://doi.org/10.5194/acp-15-305-2015

Lutsch, E., Strong, K., Jones, D. B. A., Blumenstock, T., Conway, S., Fisher, J. A., et al. (2020). Detection and attribution of wildfire pollution in the Arctic and northern midlatitudes using a network of Fourier-transform infrared spectrometers and GEOS-Chem. *Atmospheric Chemistry and Physics*, *20*(21), 12813–12851. https://doi.org/10.5194/acp-20-12813-2020

Naik, V., Voulgarakis, A., Fiore, A. M., Horowitz, L. W., Lamarque, J.-F., Lin, M., et al. (2013). Preindustrial to present-day changes in tropospheric hydroxyl radical and methane lifetime from the atmospheric chemistry and climate model intercomparison project (ACCMIP). *Atmospheric Chemistry and Physics*, *13*(10), 5277–5298. https://doi.org/10.5194/acp-13-5277-2013

NASA/LARC/SD/ASDC. (nd). MOPITT CO gridded monthly means (near and thermal infrared radiances) v007. In *NASA Langley Atmospheric Science Data Center DAAC*. https://doi.org/10.5067/TERRA/MOPITT/MOP03JM_L3.007

Nicely, J. M., Duncan, B. N., Hanisco, T. F., Wolfe, G. M., Salawitch, R. J., Deushi, M., et al. (2020). A machine learning examination of hydroxyl radical differences among model simulations for ccmi-1. *Atmospheric Chemistry and Physics*, *20*(3), 1341–1361. https://doi.org/10.5194/acp-20-1341-2020

Nicely, J. M., Salawitch, R. J., Canty, T., Anderson, D. C., Arnold, S. R., Chipperfield, M. P., et al. (2017). Quantifying the causes of differences in tropospheric oh within global models. *Journal of Geophysical Research: Atmospheres*, *122*(3), 1983–2007. https://doi.org/10.1002/2016JD026239

Olivier, J. G., Peters, J. A., Bakker, J., Berdowski, J. J., Visschedijk, A. J., & Bloos, J. P. (2002). Applications of EDGAR. Including a description of EDGAR 3.2. Reference database with trend data for 1970-1995

Pan, X., Ichoku, C., Chin, M., Bian, H., Darmenov, A., Colarco, P., et al. (2020). Six global biomass burning emission datasets: Intercomparison and application in one global aerosol model. *Atmospheric Chemistry and Physics*, *20*(2), 969–994. https://doi.org/10.5194/acp-20-969-2020

Paton-Walsh, C., Deutscher, N. M., Griffith, D. W. T., Forgan, B. W., Wilson, S. R., Jones, N. B., & Edwards, D. P. (2010). Trace gas emissions from savanna fires in northern Australia. *Journal of Geophysical Research*, *115*(D16). https://doi.org/10.1029/2009jd013309

Paton-Walsh, C., Emmerson, K. M., Garland, R. M., Keywood, M., Hoelzemann, J. J., Huneeus, N., et al. (2022). *Key challenges for tropospheric chemistry in the Southern Hemisphere*. *Elementa: Science of the Anthropocene*, 10(1). https://doi.org/10.1525/elementa.2021.00050

Paton-Walsh, C., Emmons, L. K., & Wiedinmyer, C. (2012). Australia's Black Saturday fires—Comparison of techniques for estimating emissions from vegetation fires. *Atmospheric Environment*, *60*, 262–270. https://doi.org/10.1016/j.atmosenv.2012.06.066

Paugam, R., Wooster, M., Freitas, S., & Val Martin, M. (2016). A review of approaches to estimate wildfire plume injection height within large-scale atmospheric chemical transport models. *Atmospheric Chemistry and Physics*, *16*(2), 907–925. https://doi.org/10.5194/acp-16-907-2016

Potter, C. S., Randerson, J. T., Field, C. B., Matson, P. A., Vitousek, P. M., Mooney, H. A., & Klooster, S. A. (1993). Terrestrial ecosystem production: A process model based on global satellite and surface data. *Global Biogeochemical Cycles*, *7*(4), 811–841. https://doi.org/10.1029/93gb02725

Prinn, R. G., Weiss, R. F., Arduini, J., Arnold, T., DeWitt, H. L., Fraser, P. J., et al. (2018). History of chemically and radiatively important atmospheric gases from the advanced global atmospheric gases experiment (agage). *Earth System Science Data*, *10*(2), 985–1018. https://doi.org/10.5194/essd-10-985-2018

Prosperi, P., Bloise, M., Tubiello, F. N., Conchedda, G., Rossi, S., Boschetti, L., et al. (2020). New estimates of greenhouse gas emissions from biomass burning and peat fires using MODIS Collection 6 burned areas. *Climatic Change*, *161*(3), 415–432. https://doi.org/10.1007/s10584-020-02654-0

Randerson, J. T., Chen, Y., van der Werf, G. R., Rogers, B. M., & Morton, D. C. (2012). Global burned area and biomass burning emissions from small fires. *Journal of Geophysical Research: Biogeosciences*, *117*(G4). https://doi.org/10.1029/2012jg002128

Randerson, J. T., Thompson, M. V., Malmstrom, C. M., Field, C. B., & Fung, I. Y. (1996). Substrate limitations for heterotrophs: Implications for models that estimate the seasonal cycle of atmospheric CO_2. *Global Biogeochemical Cycles*, *10*(4), 585–602. https://doi.org/10.1029/96gb01981

Rastigejev, Y., Park, R., Brenner, M. P., & Jacob, D. J. (2010). Resolving intercontinental pollution plumes in global models of atmospheric transport. *Journal of Geophysical Research*, *115*(D2). https://doi.org/10.1029/2009jd012568

Rea, G., Paton-Walsh, C., Turquety, S., Cope, M., & Griffith, D. (2016). Impact of the New South Wales fires during October 2013 on regional air quality in eastern Australia. *Atmospheric Environment*, *131*, 150–163. https://doi.org/10.1016/j.atmosenv.2016.01.034

Reinhart, W., & Millet, D. (2011). *Implementation of the RETRO anthropogenic emission inventory into the GEOS-Chem Model*.

Rodgers, C. D., & Connor, B. J. (2003). Intercomparison of remote sounding instruments. *Journal of Geophysical Research*, *108*(D3). https://doi.org/10.1029/2002jd002299

Russell-Smith, J., Yates, C. P., Whitehead, P. J., Smith, R., Craig, R., Allan, G. E., et al. (2007). Bushfires 'down under': Patterns and implications of contemporary Australian landscape burning. *International Journal of Wildland Fire*, *16*(4), 361–377. https://doi.org/10.1071/wf07018

Seiler, W., & Crutzen, P. J. (1980). Estimates of gross and net fluxes of carbon between the biosphere and the atmosphere from biomass burning. *Climatic Change*, *2*(3), 207–247. https://doi.org/10.1007/bf00137988

Shi, Y., Matsunaga, T., Saito, M., Yamaguchi, Y., & Chen, X. (2015). Comparison of global inventories of CO_2 emissions from biomass burning during 2002–2011 derived from multiple satellite products. *Environmental Pollution*, *206*, 479–487. https://doi.org/10.1016/j.envpol.2015.08.009

Shiraishi, T., & Hirata, R. (2021). Estimation of carbon dioxide emissions from the megafires of Australia in 2019–2020. *Scientific Reports*, *11*(1). https://doi.org/10.1038/s41598-021-87721-x

Siddaway, J. M., & Petelina, S. V. (2011). Transport and evolution of the 2009 Australian Black Saturday bushfire smoke in the lower stratosphere observed by OSIRIS on Odin. *Journal of Geophysical Research*, *116*(D6). https://doi.org/10.1029/2010jd015162

Simone, N. W., Stettler, M. E. J., & Barrett, S. R. H. (2013). Rapid estimation of global civil aviation emissions with uncertainty quantification. *Transportation Research Part D: Transport and Environment*, *25*, 33–41. https://doi.org/10.1016/j.trd.2013.07.001

Sindelarova, K., Granier, C., Bouarar, I., Guenther, A., Tilmes, S., Stavrakou, T., et al. (2014). Global data set of biogenic VOC emissions calculated by the MEGAN model over the last 30 years. *Atmospheric Chemistry and Physics*, *14*(17), 9317–9341. https://doi.org/10.5194/acp-14-9317-2014

Travis, K. R., Heald, C. L., Allen, H. M., Apel, E. C., Arnold, S. R., Blake, D. R., et al. (2020). Constraining remote oxidation capacity with ATom observations. *Atmospheric Chemistry and Physics*, *20*(13), 7753–7781. https://doi.org/10.5194/acp-20-7753-2020

Travis, K. R., & Jacob, D. J. (2019). Systematic bias in evaluating chemical transport models with maximum daily 8 h average (MDA8) surface ozone for air quality applications : A case study with GEOS -Chemv9 .02. *Geoscientific Model Development*, *12*(8), 3641–3648. https://doi.org/10.5194/gmd-12-3641-2019

van Oldenborgh, G. J., Krikken, F., Lewis, S., Leach, N. J., Lehner, F., Saunders, K. R., et al. (2021). Attribution of the Australian bushfire risk to anthropogenic climate change. *Natural Hazards and Earth System Sciences*, *21*(3), 941–960. https://doi.org/10.5194/nhess-21-941-2021

van der Werf, G. R., Randerson, J. T., Giglio, L., van Leeuwen, T. T., Chen, Y., Rogers, B. M., et al. (2017). Global fire emissions estimates during 1997–2016. *Earth System Science Data*, *9*(2), 697–720. https://doi.org/10.5194/essd-9-697-2017

Wai, K. M., Wu, S., Kumar, A., & Liao, H. (2014). Seasonal variability and long-term evolution of tropospheric composition in the tropics and Southern Hemisphere. *Atmospheric Chemistry and Physics*, *14*(10), 4859–4874. https://doi.org/10.5194/acp-14-4859-2014

Wiedinmyer, C., Akagi, S. K., Yokelson, R. J., Emmons, L. K., Al-Saadi, J. A., Orlando, J. J., & Soja, A. J. (2011). The fire INventory from NCAR (FINN): A high resolution global model to estimate the emissions from open burning. *Geoscientific Model Development*, *4*, 625–641. https://doi.org/10.5194/gmd-4-625-2011

Woodhouse, M. T., Luhar, A. K., Stevens, L., Galbally, I., Thatcher, M., Uhe, P., & Molloy, S. (2015). Australian reactive-gas emissions in a global chemistry-climate model and initial results. *Air Quality and Climate Change*, *49*(4), 31–38.

Woodruff, S. D., Worley, S. J., Lubker, S. J., Ji, Z., Freeman, E. J., Berry, D. I., et al. (2011). ICOADS release 2.5: Extensions and enhancements to the surface marine meteorological archive. *International Journal of Climatology*, *31*(7), 951–967. https://doi.org/10.1002/joc.2103

Wooster, M. J. (2002). Small-scale experimental testing of fire radiative energy for quantifying mass combusted in natural vegetation fires. *Geophysical Research Letters*, *29*(21). https://doi.org/10.1029/2002gl015487

Wooster, M. J., Roberts, G., Perry, G. L. W., & Kaufman, Y. J. (2005). Retrieval of biomass combustion rates and totals from fire radiative power observations: FRP derivation and calibration relationships between biomass consumption and fire radiative energy release. *Journal of Geophysical Research*, *110*(D24). https://doi.org/10.1029/2005jd006318

Worden, H., Deeter, M., Edwards, D., Gille, J., Drummond, J., & Nédélec, P. (2010). Observations of near-surface carbon monoxide from space using mopitt multispectral retrievals. *Journal of Geophysical Research*, *115*(D18). https://doi.org/10.1029/2010jd014242

Wunch, D., Toon, G. C., Blavier, J.-F. L., Washenfelder, R. A., Notholt, J., Connor, B. J., et al. (2011). The total carbon column observing network. *Philosophical Transactions of the Royal Society A: Mathematical, Physical & Engineering Sciences*, *369*, 2087–2112. https://doi.org/10.1098/rsta.2010.0240

Yevich, R., & Logan, J. A. (2003). An assessment of biofuel use and burning of agricultural waste in the developing world. *Global Biogeochemical Cycles*, *17*(4). https://doi.org/10.1029/2002gb001952

Zeng, G., Williams, J. E., Fisher, J. A., Emmons, L. K., Jones, N. B., Morgenstern, O., et al. (2015). Multi-model simulation of CO and HCHO in the southern hemisphere: Comparison with observations and impact of biogenic emissions. *Atmospheric Chemistry and Physics*, *15*, 7217–7245. https://doi.org/10.5194/acp-15-7217-2015

Zhang, L., Jacob, D. J., Yue, X., Downey, N. V., Wood, D. A., & Blewitt, D. (2014). Sources contributing to background surface ozone in the US Intermountain West. *Atmospheric Chemistry and Physics*, *14*(11), 5295–5309. https://doi.org/10.5194/acp-14-5295-2014

Zhou, M., Langerock, B., Vigouroux, C., Sha, M. K., Hermans, C., Metzger, J.-M., et al. (2019). TCCON and NDACC xCO measurements: Difference, discussion and application. *Atmospheric Measurement Techniques*, *12*(11), 5979–5995. https://doi.org/10.5194/amt-12-5979-2019